Application of the static fluctuation approximation to the computation of the thermodynamic properties of an interacting trapped two-dimensional hard-sphere Bose gas

Asaad R. Sakhel,[1] Saleem I. Qashou,[3] Roger R. Sakhel,[2] and Humam B. Ghassib[4]
[1]*Al-Balqa Applied University, Faculty of Engineering Technology, Amman 11134, Jordan*
[2]*Department of Basic Sciences, Faculty of Information Technology, Al-Isra University, Amman 11622, Jordan*
[3]*Department of Physics, Faculty of Science and Information Technology, Zarqa Private University, Zarqa 13132, Jordan*
[4]*Department of Physics, The University of Jordan, Amman, Jordan*
(Received 19 June 2010; published 14 December 2010)

The static fluctuation approximation (SFA) is applied to compute the thermodynamic properties of a trapped two-dimensional (2D) interacting hard-sphere (HS) Bose gas in the weakly and strongly interacting regime. A mean-field approach involving a variational wave function is used to compute the mean-field energy as a function of temperature for each harmonic oscillator (HO) state plugged into the SFA technique. In the variational approach, a parameter α is introduced into the harmonic oscillator wave function in order to take into account the changes in the width when the repulsive interactions between the bosons are increased. In the weakly interacting regime, below the critical temperature, the total energy of all HO states (evaluated by our model) matches the noninteracting result very well. However, beyond the critical temperature, we "fit" our energies to the classical limit for 2D bosons in a trap by using a suitably proposed weighting function. We compare our results to earlier results of mean-field theory. Further, we evaluate the density matrix arising from correlations between the HO orbitals.

DOI: 10.1103/PhysRevA.82.063618 PACS number(s): 67.85.−d, 05.70.Ce, 03.75.Hh

I. INTRODUCTION

The trapped two-dimensional (2D) interacting Bose gas presents many challenges. The evaluation of the thermodynamic properties represents just one of these challenges. It is not a straightforward matter and usually requires path-integral Monte Carlo (PIMC) calculations. In addition, many properties of 2D trapped Bose gases have yet to be explored both experimentally and theoretically [1]; various problems remain open [2], such as the estimation of the BEC transition temperature in a 2D interacting system and the explicit relationship between superfluidity and the quasicondensate. Two-dimensional systems have generally become very interesting, thanks to the interplay between BEC and Kosterlitz-Thouless transitions and other issues [3]. It is therefore in order to develop methods for exploring such systems.

Various methods and techniques have been used to investigate the trapped 2D Bose gas. Variational methods [3,4], the classical-field simulation technique [5], path-integral Monte Carlo methods [1,6,7], as well as Hartree-Fock-Bogoliubov theory [8] have all been applied. For example, Nho and Landau [1] used a finite-temperature PIMC method and showed that BEC can form at finite temperature. In order to perform their calculations, they used only $N = 27$ hard-sphere bosons, because a larger number required an extensive amount of computational time.

In this article, our chief goal is to demonstrate an application of the static fluctuation approximation (SFA) [9,10] in an evaluation of the thermodynamic properties of a trapped, 2D hard-sphere (HS) Bose gas and to compare to the corresponding 3D properties. Comparisons are also made with corresponding 2D analytical results for the thermodynamic properties. The relative advantage of the SFA is that it can yield the thermodynamic properties of a system for a broad range of temperature in one single calculation. One can obtain easily using the SFA, the energy fluctuations, number fluctuations, and thermodynamic properties, all as functions of temperature. The SFA particularly invokes the role of the energy fluctuations in the determination of the thermodynamic properties. It essentially corrects for any approximations done in the mean-field evaluation of the energy via the energy fluctuations. This corrected energy is then incorporated into the thermodynamic potential $\ln Q$, where Q is the grand canonical partition function from which all the thermodynamic properties are evaluated. In addition, the SFA can handle a large number of particles up to $N \sim 1000$. On the other hand, in other methods such as PIMC calculations, one can obtain the thermodynamic properties for one temperature at a time only, i.e., point by point. However, the SFA is limited in that it fails at very strong interactions $g > 0.01$, whereas other methods, such as PIMC calculations, are excellent in this regard as they can deal with strongly interacting systems. The SFA works very well mainly in the weakly to strongly interacting regime up to $g = 0.01$.

Some of the properties we evaluate have been—to our knowledge—rarely addressed in the literature, such as the thermal behavior of the energy for each harmonic oscillator (HO) state m and the number fluctuations $\langle(\Delta\hat{N}_m)^2\rangle$. Another goal is to shed more light on the effects of dimensionality on such systems by comparing 2D to 3D.

We thus consider N hard-sphere bosons in a 2D harmonic trap in a broad range of temperature T. The interactions between the bosons are modelled by a δ function pseudopotential. The energies for each HO state are evaluated using many-body mean-field theory, and the thermodynamic properties are obtained using SFA in 2D, applied earlier [11] to the 3D trapped interacting Bose gas. It should be emphasized that, with the SFA method applied here, we are able to use a large number of particles, $N = 1000$. It should also be emphasized that our goal is not to provide a method for computing the energies but rather to obtain them for use in SFA. Nevertheless, the mean-field model we present gives the energies accurately in the condensate regime below the transition temperature but

requires adjustment beyond the transition temperature toward the classical regime, as will be shown later.

In our previous publication [11], we evaluated the thermodynamic properties of the 3D trapped HS Bose gas. The HO wave function was employed:

$$\phi_n(x) = \frac{1}{\sqrt{2^n\sqrt{\pi}n!}} \exp(-x^2/2) H_n(x), \quad (1)$$

whose width was invariant with the change in the HS repulsion. This gave reasonable results in the weakly interacting regime; but the evaluation of the properties failed in the strongly interacting regime. It is known that, at the larger HS repulsion, the wave function of a trapped Bose gas broadens significantly to several trap lengths. This has been observed in other well-established methods, such as the quantum variational Monte Carlo method [12,13]. On going to stronger repulsive forces, our previous numerical minimization technique for the function

$$f(\mu,T) = \left\{ N - \sum_{m=0}^{M} \frac{d_m}{\exp[(\langle E_m\rangle - \mu)\beta] - 1} \right\}^2 \quad (2)$$

failed to yield the correct chemical potential $\mu(T)$ when the interactions were increased beyond $g = 1 \times 10^{-3}$, where g is the two-body interaction parameter and T the temperature. In Eq. (2), N is the total number of particles, d_m the degeneracy of HO state m, $\langle E_m\rangle$ the average energy, $\beta = 1/(k_B T)$, k_B being Boltzmann's constant, and M the total number of HO states. This failure may be attributed to the incorrect behavior of the energies presumably resulting from the invariance of the width of the wave function (1) with g. It was observed that the SFA failed at strong interactions of the order $g = 1 \times 10^{-2}$. In the present investigation, we try to deal with the latter issue, albeit for a trapped 2D interacting HS Bose gas, using a mean-field (MF) variational approach. We therefore propose to use a parameterized form of Eq. (1):

$$\phi_n(x,\alpha) = \frac{\alpha^{1/4}}{\sqrt{2^n\sqrt{\pi}n!}} \exp(-\alpha x^2/2) H_n(\sqrt{\alpha}x), \quad (3)$$

where α is a variational parameter. This wave function is normalized to 1 via the coefficient $\alpha^{1/4}/\sqrt{2^n\sqrt{\pi}n!}$. The inclusion of α makes the wave function flexible to variations in the repulsive forces between the bosons.

Our key results are as follows. We find that the SFA is able to reproduce the thermodynamic properties of a 2D trapped HS Bose gas in the weakly interacting regime. It is found that the specific heat capacity displays a phase transition, indicating a possible true condensation in the zero-momentum state. A macroscopic occupation of the zero-HO state is displayed by the Bose-Einstein occupancy, and the number fluctuations reveal some interesting features. Further, the 3D entropy is smaller than the 2D one. The 2D internal energy and pressure are larger than their 3D counterparts. At large repulsive interactions, the 2D zero-HO state is depleted significantly more than at a comparable interaction strength in 3D. Hence, there are substantial differences between the thermodynamic properties of the 2D and 3D cases, indicating again that they are very distinct systems.

Previous theoretical work on the 2D Bose gas, whether trapped [1–8,14–19] or uniform [20], is abundant. For example, Pearson *et al.* [7] calculated finite-temperature properties of 1000 hard-core bosons in an isotropic 2D HO potential using PIMC calculations. The system that they were trying to simulate was strictly 2D. They found that the transition temperature decreases with increasing hard-core diameter; that is, as the number of particles increases, very small values of the s-wave scattering length a_s are required to avoid total depletion of the condensate; and the difference between ideal and interacting Bose gases virtually disappears if the range of interactions is small enough.

One major point in the literature is the question of whether one could observe a true condensate in a 2D trapped interacting Bose gas. For example, the trapped interacting 2D Bose gas was investigated as early as 1997 when Mullin [19] found that, in the thermodynamic limit, there is no BEC in the $k = 0$ momentum state for the 2D harmonic oscillator; but BEC does exist in the lowest harmonic oscillator state, $m = 0$. Afterward, Heinrichs and Mullin [6] investigated the behavior of harmonic Bose systems in 2D using PIMC calculations. It was found that, for a 2D Bose gas in the thermodynamic limit, there is no phase transition to a Bose-condensed state, even in a trap. Nevertheless, they stated that there should be a macroscopic fraction of particles in the ground state at finite temperature when the number of particles is finite. In other investigations, Bayindir and Tanatar [14] found, by employing the two-fluid model, that BEC may occur in 2D traps if the short-range interactions are not too strong. Gies *et al.* [8] showed that a trapped 2D dilute Bose gas can undergo BEC below a transition temperature. Recently, Hadzibabik *et al.* [18] found that, in 2D, long-range order is destroyed by thermal fluctuations at any finite temperature, both in an ideal and an interacting Bose gas. In addition, the trapped quasi-2D Bose gas [1,5,17,18] and the equation of state of a weakly interacting, homogeneous 2D Bose gas [20] have been considered.

The article is organized as follows. In Sec. II, we outline the method used. In Sec. III, we analyze the SFA in 2D. In Sec. IV, we present our results, where we make comparisons with our previous 3D results. In Sec. V, we discuss density matrices of HO orbitals. Finally, in Sec. VI, we present our discussion and conclusions.

II. METHOD

A. Mean-field energies

We start with computing the mean-field energies for the SFA using the form given by Eq. (3). Specifically, we calculate the mean-field energy for each HO state. This works well for temperatures less than the critical temperature T_c; however, beyond T_c, our energies are lower than the classical limit. In this latter regime, then, it was necessary to readjust the energies by "fitting" them to the classical regime via a "weighting function." This was necessary in view of our limited computational capabilities which precluded the evaluation of $n!$ in Eq. (3) for $n > 150$, and therefore we were restricted to $M = 150$ states. As was done previously, we begin by substituting Eq. (3) into the two-dimensional many-body Hamiltonian in second quantization which, in units of the trap

($\hbar\omega_{\rm HO}$), reads:

$$\hat{H} = \int d^2\mathbf{r}\hat{\psi}^\dagger(\mathbf{r})\left[-\frac{1}{2}\nabla^2 + V_{\rm ext}(\mathbf{r})\right]\hat{\psi}(\mathbf{r}) + \frac{1}{2}\int d^2\mathbf{r}\hat{\psi}^\dagger(\mathbf{r})\hat{\psi}^\dagger(\mathbf{r}')V_{\rm int}(\mathbf{r}-\mathbf{r}')\hat{\psi}(\mathbf{r}')\hat{\psi}(\mathbf{r}), \quad (4)$$

where

$$\hat{\psi}(\mathbf{r}) \equiv \sum_n \hat{b}_n\phi_n(\mathbf{r},\alpha) \quad (5)$$

are the field operators, with $\hat{b}_n$ ($\hat{b}_n^\dagger$) the bosonic creation (annihilation) operators, and

$$\phi_n(\mathbf{r},\alpha) = \phi_{n_x}(x,\alpha)\phi_{n_y}(y,\alpha) \quad (6)$$

are the single-particle wave functions with $n = n_x + n_y$. $V_{\rm ext}(\mathbf{r}) = (1/2)r^2$ is the external harmonic trap where $r^2 = x^2 + y^2$. It is then straightforward to evaluate the noninteracting part of the Hamiltonian:

$$\hat{H}_0 = \sum_{m=0}^{M}\hat{E}_m^{(0)}\hat{N}_m, \quad (7)$$

where $\hat{E}_m^{(0)}$ is the noninteracting energy operator, $\hat{N}_m = \hat{b}_m^\dagger\hat{b}_m$ is the number operator, and M is the total number of states used. For our present purposes, we define $u = \sqrt{\alpha}x$ and $v = \sqrt{\alpha}y$. Then we employ the recursion relation [21]

$$H_m''(u) = 2u\,H_m'(u) - 2m\,H_m(u), \quad (8)$$

the orthogonality relation for the Hermite functions

$$\int_{-\infty}^{+\infty} du\, e^{-u^2}H_n(u)H_m(u) = 2^n\sqrt{\pi}n!\delta_{n,m}, \quad (9)$$

and the relation

$$\int_{-\infty}^{+\infty} u^2e^{-u^2}H_n^2(u)\,du = \sqrt{\pi}\,2^n\,n!\left(n+\frac{1}{2}\right) \quad (10)$$

in the evaluation of the many-body Hamiltonian (4). After some straightforward algebra one arrives at

$$\hat{H}_0 = \sum_{m=0}^{M}\left(\frac{\alpha}{2}+\frac{1}{2\alpha}\right)(m+1)\,\hat{b}_m^\dagger\hat{b}_m. = \sum_{m=0}^{M}\hat{E}_m^{(0)}\hat{b}_m^\dagger\hat{b}_m. \quad (11)$$

The noninteracting energy $\hat{E}_m^{(0)}$ can then be obtained, as usual, from the commutation relation

$$[\![\hat{b}_m,[\hat{H}_0,\hat{b}_m]]\!] = \hat{E}_m^{(0)}, \quad (12)$$

which leads to the expectation value

$$\langle\hat{E}_m^{(0)}\rangle = \left(\frac{\alpha}{2}+\frac{1}{2\alpha}\right)(m+1). \quad (13)$$

The parameterized interacting part of the Hamiltonian $\hat{H}_1$ is obtained after substituting Eq. (5) into the second term on the right-hand side of Eq. (4) and using a δ function pseudopotential for the pair interaction:

$$V_{\rm int}(\mathbf{r}-\mathbf{r}') = g\delta(\mathbf{r}-\mathbf{r}'), \quad (14)$$

where g is the interaction parameter in 2D. This leads to

$$\hat{H}_1 = \frac{g}{2}\sum_{c_1c_2c_3c_4}\hat{b}_{c_1}^\dagger\hat{b}_{c_2}^\dagger\hat{b}_{c_3}\hat{b}_{c_4} \times\int\phi_{c_1}^*(\mathbf{r},\alpha)\phi_{c_2}^*(\mathbf{r},\alpha)\phi_{c_3}(\mathbf{r},\alpha)\phi_{c_4}(\mathbf{r},\alpha)\,d^2\mathbf{r}, \quad (15)$$

where c_i are integers representing the HO states. Using the same commutator (12) and substituting the forms for $\phi_n(\mathbf{r},\alpha)$ [Eq. (3)], we get the expectation value of the interacting part of the energy, $\langle\hat{E}_m^{(1)}\rangle$, in a manner similar to the method outlined in Ref. [11]:

$$\langle[\![\hat{b}_m,[\hat{H}_1,\hat{b}_m]]\!]\rangle = \langle\hat{E}_m^{(1)}\rangle = \frac{1}{2}g\sum_{n=0}^{M}\tilde{c}^{\rm 2D}(n,m)\langle\hat{N}_n\rangle, \quad (16)$$

where

$$\langle\hat{N}_m\rangle = \frac{d_m}{e^{\beta(\langle\hat{E}_m^{(0)}\rangle-\mu)}-1} \quad (17)$$

is the occupancy of state m and $d_m = (m+1)$. Initially, $\langle\hat{N}_m\rangle$ is evaluated with $\langle\hat{E}_m^{(0)}\rangle = (m+1)$ (i.e., $\alpha = 1$) for the noninteracting case and subsequently employed in Eq. (16). After evaluating the interacting energies, Eq. (22) below is used to calculate $\langle\hat{N}_m\rangle$ for the interacting case. The interaction matrix $\tilde{c}^{\rm 2D}(n,m)$ in 2D resulting from the use of Eq. (3) is given by

$$\tilde{c}^{\rm 2D}(n,m) = \frac{1}{d_m}\sum_{\substack{n_x,n_y,n_z\\ m_x,m_y,m_z}}\prod_{i=1}^{2}\left[B_{n_i,m_i}\alpha\int_{-\infty}^{+\infty}\exp\left(-2\alpha x_i^2\right) \times H_{n_i}^2(\sqrt{\alpha}x_i)H_{m_i}^2(\sqrt{\alpha}x_i)dx_i\right], \quad (18)$$

where $x_1 = x$, $x_2 = y$, $m = m_x + m_y$, $n = n_x + n_y$, and

$$B_{n_i,m_i} = \frac{1}{2^{n_i+m_i}\,n_i!m_i!\pi}. \quad (19)$$

Substituting $x_i = u_i/\sqrt{\alpha}$, we recover the same form of Eq. (12) in Ref. [11], but for 2D and with an additional factor of α, that is,

$$\tilde{c}^{\rm 2D}(n,m) = \alpha c^{\rm 2D}(n,m), \quad (20)$$

where $c^{\rm 2D}(n,m)$ is given by

$$c^{\rm 2D}(n,m) = \frac{1}{d_m}\sum_{\substack{n_x,n_y,n_z\\ m_x,m_y,m_z}}\prod_{i=1}^{2} \times\left[B_{n_i,m_i}\int_{-\infty}^{+\infty}\exp\left(-2u_i^2\right)H_{n_i}^2(u_i)H_{m_i}^2(u_i)\,du_i\right]. \quad (21)$$

Eventually, the total energy $\langle\hat{E}_m\rangle$ in 2D for each state m can be written

$$\langle\hat{E}_m\rangle = \left[\frac{\alpha}{2}+\frac{1}{2\alpha}\right](m+1) + \frac{1}{2}g\alpha\sum_{n=0}^{M}c^{\rm 2D}(n,m)\langle\hat{N}_n\rangle, \quad (22)$$

and the total energy of the system is given by a sum over all states:

$$E_{\text{total}} = \sum_{m=0}^{M} \langle \hat{E}_m \rangle \langle \hat{N}_m \rangle. \tag{23}$$

It is shown later in Sec. IV B that Eq. (23) reproduces the energies below the critical temperature reasonably well. However, beyond the critical temperature and because of a restricted number of states M, the energies lie lower than the classical limit. To obtain correct energies $\langle \hat{E}_m \rangle$ in the classical limit, we propose multiplying Eq. (23) by a "weighting function" $w(T)$ given by

$$w(T) = \begin{cases} 1, & T \leqslant T_c \\ (T/T_c)^{\gamma}, & T > T_c \end{cases}, \tag{24}$$

where γ is an adjustable parameter. Hence γ is "fitted" to the energies in the classical regime. This is done only for mathematical convenience so as to enable us to use correct values for $\langle \hat{E}_m \rangle$ in the SFA.

B. Variational optimization

In this section, we demonstrate how to obtain the optimal variational parameter α as a function of g and T. The importance of α is revealed later. To optimize α, we differentiate Eq. (23) with respect to α and set the resulting derivative equal to zero. With some considerations to be discussed below, this gives a compact form for the optimized α. We begin with

$$\left.\frac{\partial E_{\text{total}}}{\partial \alpha}\right|_{\alpha=\alpha_0} = \left[\frac{1}{2} - \frac{1}{2\alpha^2}\right] \sum_{m=0}^{M} (m+1) \langle \hat{N}_m \rangle + \frac{1}{2} g \sum_{m=0}^{M} \sum_{n=0}^{M} c^{2\text{D}}(n,m) \langle \hat{N}_n \rangle \langle \hat{N}_m \rangle \Big|_{\alpha=\alpha_0} = 0. \tag{25}$$

After a little algebra one gets

$$\alpha_0^2 = \frac{\sum_{m=0}^{M} (m+1) \langle \hat{N}_m \rangle}{\sum_{m=0}^{M} \left[(m+1) \langle \hat{N}_m \rangle + g \sum_{n=0}^{M} c^{2\text{D}}(n,m) \langle \hat{N}_n \rangle \langle \hat{N}_m \rangle \right]}, \tag{26}$$

which shows that the optimal $\alpha = \alpha_0$ depends on the temperature, number of states M, and the interaction strength. It is noted that, although E_{total} is multiplied by $w(T)$ [Eq. (24)] above, the same result (26) is obtained as without $w(T)$. In the previous investigations of trapped HS Bose gases [12,13], α was varied only as a function of the interaction at zero temperature. Now α is varied additionally with T; one can show the thermal effect on the broadening as T is increased. One might argue that the derivative of Eq. (25) should also contain derivatives of the occupancy function, that is,

$$\frac{\partial \langle \hat{N}_k \rangle}{\partial \alpha} = -\frac{\beta d_k \left(\dfrac{\partial \langle \hat{E}_k \rangle}{\partial \alpha} - \dfrac{\partial \mu}{\partial \alpha} \right) e^{\beta(\langle \hat{E}_k \rangle - \mu)}}{[e^{\beta(\langle \hat{E}_k \rangle - \mu)} - 1]^2}. \tag{27}$$

It follows that, according to (22), $\partial \langle \hat{E}_k \rangle / \partial \alpha$ in (27) should contain another derivative of the occupancy $\partial \langle \hat{N}_k \rangle / \partial \alpha$, which in turn yields another $\partial \langle \hat{E}_k \rangle / \partial \alpha$, and so on! Thus, at first glance, it looks that $\partial \langle \hat{E}_k \rangle / \partial \alpha$ is an infinitely differentiable quantity with respect to α. However, if one considers the normalization condition

$$N = \sum_{k=0}^{M} \frac{d_k}{e^{\beta(\langle \hat{E}_k \rangle - \mu)} - 1}, \tag{28}$$

then the constancy of N implies that

$$\frac{\partial N}{\partial \alpha} = 0 = \sum_{k=0}^{M} \frac{\partial \langle \hat{N}_k \rangle}{\partial \alpha} = -\beta \sum_{k=0}^{M} d_k \frac{\left(\dfrac{\partial \langle \hat{E}_k \rangle}{\partial \alpha} - \dfrac{\partial \mu}{\partial \alpha} \right) e^{\beta(\langle \hat{E}_k \rangle - \mu)}}{[e^{\beta(\langle \hat{E}_k \rangle - \mu)} - 1]^2}. \tag{29}$$

Hence, one can take $\partial \langle \hat{N}_k \rangle / \partial \alpha = 0$ and there would be no need to further differentiate the occupancy with respect to α in Eq. (25). Further, one obtains $\sum_{k=0}^{M} d_k (\partial \langle \hat{E}_k \rangle / \partial \alpha) e^{\beta(\langle \hat{E}_k \rangle - \mu)} = (\partial \mu / \partial \alpha) \sum_{k=0}^{M} d_k e^{\beta(\langle \hat{E}_k \rangle - \mu)}$.

C. The SFA iterative procedure

In this section, we outline again briefly the iterative procedure used to compute the energy fluctuations $\varphi_F(m,T) = [\langle (\Delta E)^2 \rangle]^{1/2}$ used in the SFA method [11]. The main goal is to solve Eq. (34) below for $\varphi_F(m,T)$ via a loop over all temperatures T. But first, let us recall the following important SFA equations used in the iterative procedure:

$$\begin{aligned} \eta_0(m,T) &\equiv \frac{1}{2} \left\{ \frac{1}{\exp[\beta(\langle \hat{E}_m \rangle - \mu + \varphi_m)] - 1} + \frac{1}{\exp[\beta(\langle \hat{E}_m \rangle - \mu - \varphi_m)] - 1} \right\}; \\ \eta_1(m,T) &\equiv \frac{1}{2\varphi_m} \left\{ \frac{1}{\exp[\beta(\langle \hat{E}_m \rangle - \mu + \varphi_m)] - 1} - \frac{1}{\exp[\beta(\langle \hat{E}_m \rangle - \mu - \varphi_m)] - 1} \right\}. \end{aligned} \tag{30}$$

The procedure is then as follows: (i) One begins by initializing the fluctuations $\varphi_F(m,T)$ and "true" correlations between the number fluctuations $\langle \Delta \hat{N}_m \Delta \hat{N}_k \rangle_c$ for $m \neq k$ and all values of m and k up to a certain limit M. Next, one starts a loop aimed at optimizing $\varphi_F(m,T)$ and $\langle \Delta \hat{N}_m \Delta \hat{N}_k \rangle_c$ for $m \neq k$. (ii) At the beginning of each iteration, $f(\mu,T)$ given by Eq. (2) is minimized with respect to $\mu(T)$ at each T in a range of T. (iii) The resulting $\mu(T)$ is used to compute the square of the number fluctuations $\langle (\Delta \hat{N}_m)^2 \rangle$, which is computed from

$$\langle (\Delta \hat{N}_m)^2 \rangle = \eta_0(m,T)[1 + \eta_0(m,T)] + \eta_1(m,T) g \sum_{k \neq m}^{M} \tilde{c}^{2\text{D}}(m,k) \langle \Delta \hat{N}_k \Delta \hat{N}_m \rangle_c, \tag{31}$$

where $\eta_0(m,T)$ and $\eta_1(m,T)$ are given above by Eq. (30), and $\tilde{c}^{2\text{D}}(m,k)$ is the two-dimensional interaction matrix obtained from Eqs. (20) and (21). (iv) Subsequently, the ordinary

correlations between the number fluctuations $\langle \Delta\hat{N}_m \Delta\hat{N}_k \rangle$ for $m \neq k$ are updated using $\langle (\Delta\hat{N}_m)^2 \rangle$ in

$$\langle \Delta\hat{N}_m \Delta\hat{N}_k \rangle = \langle (\Delta\hat{N}_m)^2 \rangle \delta_{m,k} + \langle \Delta\hat{N}_m \Delta\hat{N}_k \rangle_c. \quad (32)$$

(v) The "true" correlations are updated using the latter $\langle \Delta\hat{N}_m \Delta\hat{N}_k \rangle$ according to

$$\langle \Delta\hat{N}_m \Delta\hat{N}_k \rangle_c = \eta_1(m,T) g \sum_{i \neq m}^{M} \tilde{c}^{2D}(m,i) \langle \Delta\hat{N}_i \Delta\hat{N}_k \rangle. \quad (33)$$

(vi) Then, the energy fluctuations are computed using the updated $\langle \Delta\hat{N}_m \Delta\hat{N}_k \rangle_c$ via

$$[\varphi_F(m,T)]^2 = \frac{g}{\eta_1(m,T)} \sum_{i \neq m}^{M} \tilde{c}^{2D}(m,i) \langle \Delta\hat{N}_i \Delta\hat{N}_m \rangle_c. \quad (34)$$

(vii) One then returns to step (iii) using the updated $\varphi_F(m,T)$ and $\langle \Delta\hat{N}_m \Delta\hat{N}_k \rangle_c$ and repeats steps (iii)–(vii) for a specified number of iterations. (viii) When the total number of iterations has been reached, the procedure increments the temperature by a step ΔT and the whole procedure is repeated from steps (ii)-(viii).

III. ANALYSIS

In this section, we analyze the SFA method in 2D in a manner similar to Ref. [11]. The goal is again to show the stability of the solutions and the thermal behavior of the energy fluctuations; this time in 2D. The variational parameter α of Eq. (3) is also addressed and reveals a strong dependence on both T and g.

A. The variational parameter α

Figure 1 displays α versus T (i.e., T/T_c on a $\log_{10}$ scale) for several values of the interaction parameter g: (open triangles) $g = 1 \times 10^{-4}$, (solid circles) 1×10^{-3}, (open circles) 1×10^{-2}, (solid squares) 5×10^{-2}, (open squares) 1×10^{-1}, (stars) 5×10^{-1}. The same labels are used in all figures containing g, except where indicated otherwise. The system is a 2D trapped HS Bose gas of $N = 1000$ particles, $M = 150$ states, at a trapping frequency of $\omega_{HO} = 2\pi \times 10$ Hz. T_c is the critical temperature for noninteracting bosons in a 2D trap given by

$$T_c^{2D} = \frac{\hbar\omega_{HO}}{k_B} \frac{\sqrt{6}}{\pi} N^{1/2}. \quad (35)$$

For $N = 1000$, this has the value 11.833 nK, which is used throughout this article, except where indicated otherwise.

One can see that α rises with T asymptotically, approaching the value 1. That is, the width of the wave function decreases with increasing temperature until α reaches 1 and stops changing. Note that, whereas for $g < 0.5$ the value α comes close to 1 at $T/T_c \sim 9$, for $g = 0.5$, however, $\alpha \to 0.9$ as $T \to \infty$. Thus, as the HS diameter (i.e., repulsion) rises, the value of α drops further below 1 as $T \to \infty$. The behavior of α vs. T in Fig. 1 then differs for $g = 0.5$ than for the rest of the $g < 0.5$: α approaches 0.9 instead of 1 as $T \to \infty$. In order to explain the reason for this difference, one needs to inspect Eq. (26) a little closer. For this purpose, we plot the

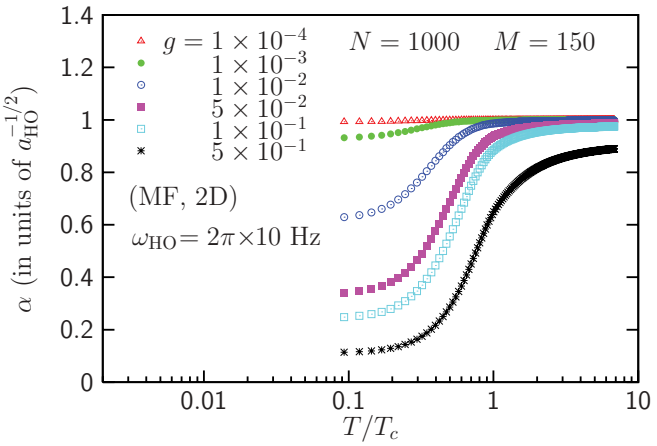

FIG. 1. (Color online) Mean-field (MF) variational parameter α of Eq. (3) as a function of temperature (T/T_c in the $\log_{10}$ scale) at various interaction strengths g. The system is a 2D trapped interacting hard sphere Bose gas of $N = 1000$ particles, $M = 150$ states, and a trapping frequency of $\omega_{HO} = 2\pi \times 10$ Hz. $T_c = 11.833$ nK is the 2D result for the critical temperature. (Open triangles) $g = 1 \times 10^{-4}$; (solid circles) $g = 1 \times 10^{-3}$; (open circles) $g = 1 \times 10^{-2}$; (solid squares) $g = 5 \times 10^{-2}$; (open squares) $g = 1 \times 10^{-1}$; and (stars) $g = 5 \times 10^{-1}$.

two parts of the denominator in Eq. (26) as functions of T in Fig. 2; that is, we define and plot

$$\langle E_{\text{nonint}} \rangle = \sum_{m=0}^{M} (m+1) \langle \hat{N}_m \rangle \quad (36)$$

(down triangles) and

$$\langle I_{\text{int}} \rangle = \sum_{m=0}^{M} \sum_{n=0}^{M} c^{2D}(n,m) \langle \hat{N}_n \rangle \langle \hat{N}_m \rangle \quad (37)$$

(solid circles), where for $N = 1000$, $M = 150$, and $T \to \infty$, the value of $\langle I_{\text{int}} \rangle \to (\sim 2.2 \times 10^4)$ as displayed in Fig. 2

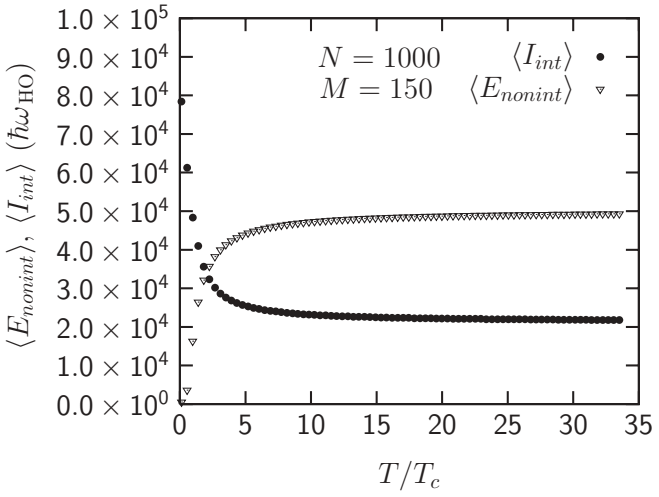

FIG. 2. Temperature behavior of Eqs. (36) (down triangles) and (37) (solid circles) displaying the limit of $T \to \infty$. The system is a 2D harmonically trapped Bose gas of $N = 1000$ particles and $\omega_{HO} = 2\pi \times 10$ Hz trapping frequency.

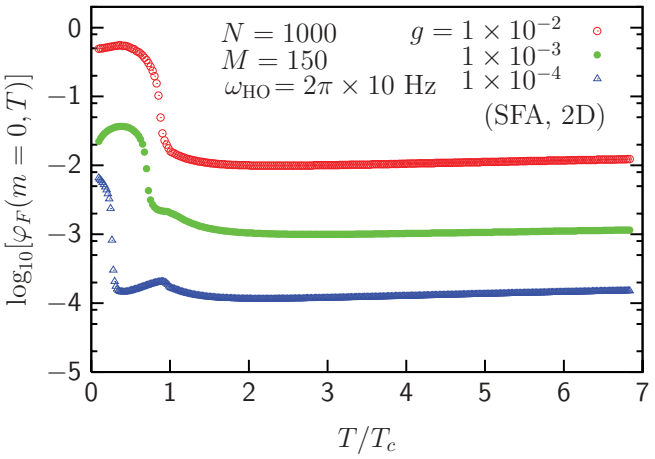

FIG. 3. (Color online) SFA energy fluctuations $\varphi_F(m=0,T)$ {i.e., $\log_{10}[\varphi_F(m=0,T)]$} as a function of T for the same system of Fig. 1 and the given values of g. (Open circles) $g = 1 \times 10^{-2}$; (solid circles) $g = 1 \times 10^{-3}$; and (open triangles) $g = 1 \times 10^{-4}$. ϕ_F is in units of $\hbar\omega_{HO}$.

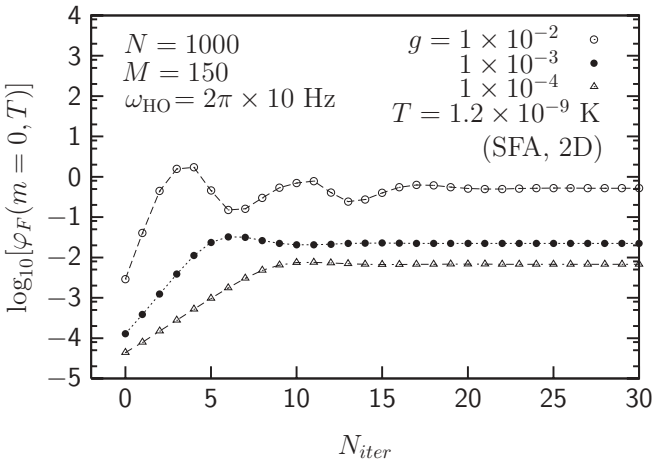

FIG. 4. SFA energy fluctuations $\phi_F(m=0,T)$ {i.e., $\log_{10}[\phi_F(m=0,T)]$} as a function of the number of iterations for the same systems in Fig. 3 at $T = 1.2 \times 10^{-9}$ K. The same legends are used as in Fig. 3.

which extends up to $T/T_c = 34$; that is, $\langle I_{\rm int}\rangle$ goes to a well-defined limit in the high-temperature regime regardless of the value of g. Further, $\langle E_{\rm nonint}\rangle \to (\sim 5 \times 10^4)$ when $T \to \infty$. This is because $\langle \hat{N}_k\rangle$ in (37) is independent of g since they are the occupancies for a noninteracting system, and the matrix $c^{2D}(n,m)$ given by Eq. (21) is always the same and independent of T and g. It is only when $\langle I_{\rm int}\rangle$ is multiplied by g that the interactions change with g. For $g < 0.5$, such as $g = 0.1$, one can use (26) to estimate the $T \to \infty$ limit of α to be simply $\sim\sqrt{5 \times 10^4/(5 \times 10^4 + g \times 2.2 \times 10^4)} = 0.98$, i.e., it approaches 1. Note that one simply multiplies the limit of $\langle I_{\rm int}\rangle$ by g. Consequently, the same estimate leads to $\sim\sqrt{5 \times 10^4/(5 \times 10^4 + g \times 2.2 \times 10^4)} = 0.905$ for $g = 0.5$, i.e., it does not approach 1. In comparison, the thermal de Broglie wavelength decreases with increasing T as well, until, beyond the transition temperature, the system enters the classical regime. By analogy, the thermal de Broglie wavelength is indirectly described by α. In conjunction, the transition from the quantum to the classical regime might also be described by α. Indeed, when $\alpha \to 1$ asymptotically, the size of the bosons $\to$ constant, as they become now classical particles whose size is constant with temperature.

B. Fluctuations

Figure 3 displays the SFA energy fluctuations for the lowest HO state $\log_{10}[\phi_F(m=0,T)]$ as a function of temperature at several values of g. The system is the same as in Fig. 1. Here, ϕ_F for $g > 1 \times 10^{-4}$ has maxima at $T < T_c$, and beyond them $\phi_F(m=0,T)$ decreases steeply with T in the lower-temperature regime $T/T_c < 1$, until it becomes constant at higher temperatures, $T/T_c \gg 1$. This behavior for ϕ_F differs remarkably from that in the 3D regime displayed in Fig. 2 of our previous publication [11]. It can also be seen that ϕ_F generally increases with increasing g.

C. Stability of the solutions

Here, we check again the convergence of the SFA iterations. The same systems as in Fig. 3 are considered. Figures 4 and 5 display $\log_{10}[\phi_F(m=0,T)]$ for $T = 1.2 \times 10^{-9}$ K and 3.0×10^{-8} K, respectively. Figures 6 and 7 are the same, except for the HO state $m = 1$. Again, all these figures reveal that the SFA converges after a relatively small number of iterations, $N_{\rm iter}$. Thus, we can safely say that the SFA is applicable to 2D. Further, the SFA at $T = 3.0 \times 10^{-8}$ K converges almost immediately, i.e., after 1 or 2 iterations; whereas at $T = 1.2 \times 10^{-9}$ K it takes 15–20 iterations for convergence. Thus, for lower temperatures in the nanokelvin regime, a larger number of iterations is required to obtain a stable solution.

D. Convergence of a physical quantity with M

In what follows, we check whether $M = 150$ is enough to achieve reasonable convergence of an estimated quantity, such as the energy. For this purpose, we display in Fig. 8 the total energy $E_{\rm total}$ [Eq. (23) multiplied by $\hbar\omega_{HO}/(Nk_BT_c)$]

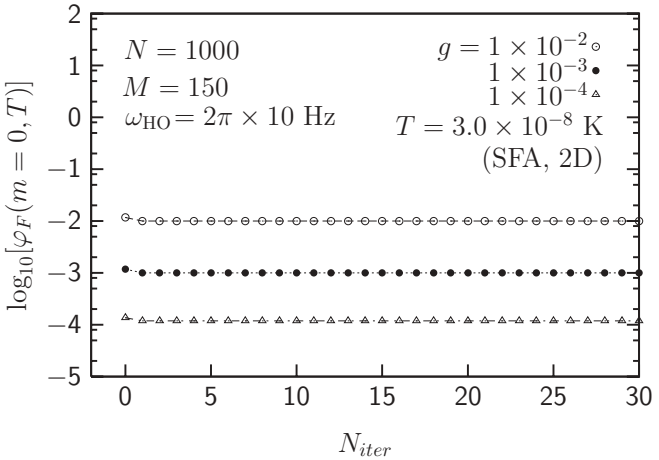

FIG. 5. As in Fig. 4; but at $T = 3.0 \times 10^{-8}$ K.

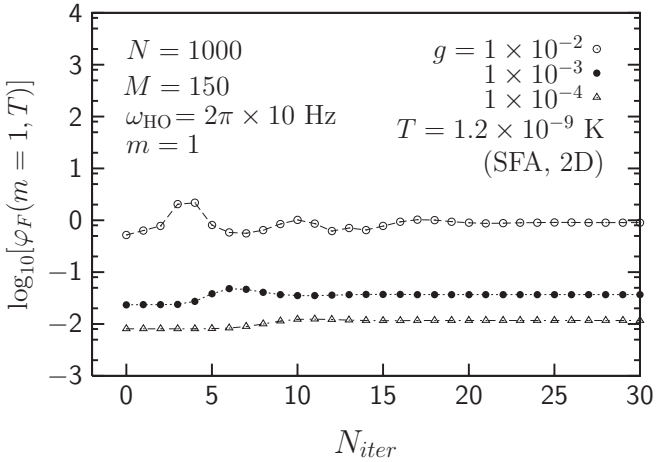

FIG. 6. As in Fig. 4; but for HO state $m = 1$.

as a function of M and at the indicated temperatures T: (open circles) $T = 0.3T_c$, (solid circles) $0.7T_c$, (open triangles) $1.0T_c$, and (solid triangles) $1.5T_c$. The system is a 2D harmonically trapped hard sphere Bose gas of $N = 1000$ and $g = 1 \times 10^{-3}$. One can see that $M = 150$ is enough for E_{total} to be a convergent quantity up to the transition temperature T_c. In fact, the convergence for $T \leqslant T_c$ begins already at $M = 120$. For $T > T_c$, clearly a larger number M is needed. But since we "fit" the energies beyond T_c to the classical limit using a "weighting" function $w(T)$ given by Eq. (24), we do not need to worry about M being large enough or not beyond the transition. What matters, is only the condensate regime. Another question was whether the values of $c^{2D}(n,m)$ are really significant beyond 150 states; that is, we needed to check whether the matrix elements $c^{2D}(n > 150,m)$ or $c^{2D}(n,m > 150)$ have really any significant effect on the convergence of a physical quantity. This was done by computing the energies in the presence of a cutoff introduced into the interactions, i.e., by setting $c^{2D}(n,m > 150) = 0$ and $c^{2D}(n > 150,m) = 0$. Our concentration was particularly on the low-temperature regime below T_c. In Fig. 8 the effect of the latter setting is displayed by the "times" labels for $T = 1.0T_c$ (cutoff). One can see that the data obtained by using

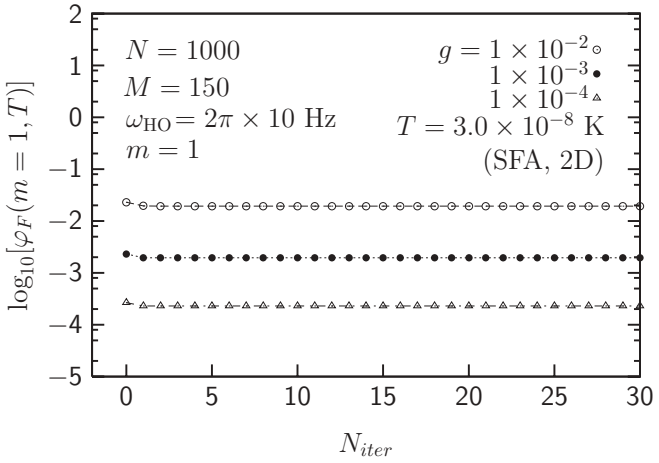

FIG. 7. As in Fig. 5 but for $m = 1$.

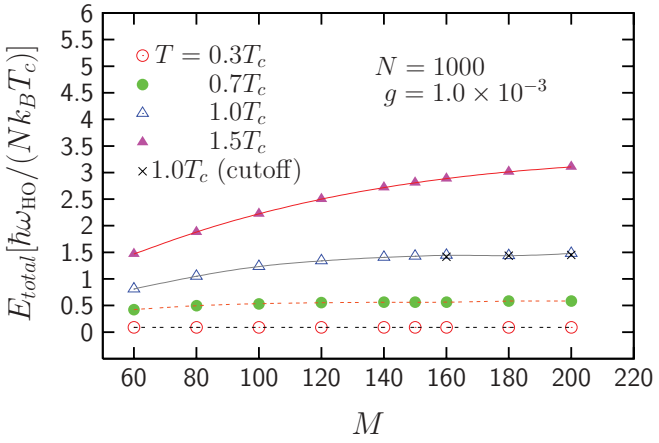

FIG. 8. (Color online) Convergence of the total energy E_{total} [multiplied by $\hbar\omega_{\text{HO}}/(Nk_BT_c)$] with the total number of states M at several temperatures T. The system is a 2D harmonically trapped hard sphere Bose gas of $N = 1000$ and $g = 1 \times 10^{-3}$. (Open circles) $T = 0.3T_c$, where T_c is the transition temperature. (Solid circles and open triangles) $0.7T_c$ and $1.0T_c$, respectively. (Solid triangles) Temperature above the transition, $1.5T_c$. (Xs) Special case for $M > 150$ when a cutoff in the interactions is present, i.e., $c^{2D}(n > 150,m) = c^{2D}(n,m > 150) = 0$.

a cutoff (times) are indistinguishable from the data without a cutoff (open triangles), i.e., by using values for $c^{2D}(n,m)$ beyond 150 states. The reason is because the occupancies $\langle\hat{N}_m\rangle$ are very small for the higher m in the low-temperature regime; in fact $\lim_{m\to\infty}\langle\hat{N}_m\rangle = 0$ for $T \leqslant T_c$. Therefore, the magnitude of the summands $c^{2D}(n,m)\langle\hat{N}_n\rangle\langle\hat{N}_m\rangle$ in (37) become very small compared to the $(m+1)\langle\hat{N}_m\rangle$ in (36) for m or n exceeding 150. It is thus concluded that the role of the higher states is very much undermined in the condensate regime.

IV. RESULTS

In our previous work [11], we explained why we were not able to introduce more than $M = 100$ states in our three-dimensional calculations. This was because the computation required to evaluate the 3D interaction matrix $c(k,m)$ for more than 100 states was very expensive. Even in the present two-dimensional case, although we were able to reach 150 states, the computational time required was substantial. In fact, our computer was not able to evaluate the factorial of n for HO states $n > 150$ needed in the normalization of the HO wave function, Eq. (3). This remains a technical problem that one needs to solve. In any case, our focus is not on the evaluation of the energies.

A. Chemical potential

Figure 9 displays the MF chemical potential $\mu(T)$ as a function of T for several values of g. [Note the new label $g = 2 \times 10^{-1}$ (times).] The system is the same as in Fig. 3, and $\mu(T)$ was obtained by the same technique previously outlined in Ref. [11]. For $g \leqslant 1 \times 10^{-3}$, $\mu(T)$ is constant at $T < T_c$ and decreases almost linearly at $T > T_c$. For $g > 1 \times 10^{-3}$, a small bump develops around T_c; but then $\mu(T)$ decreases again with increasing T. One can see that $\mu(T)$ in 2D from $T/T_c = 1$

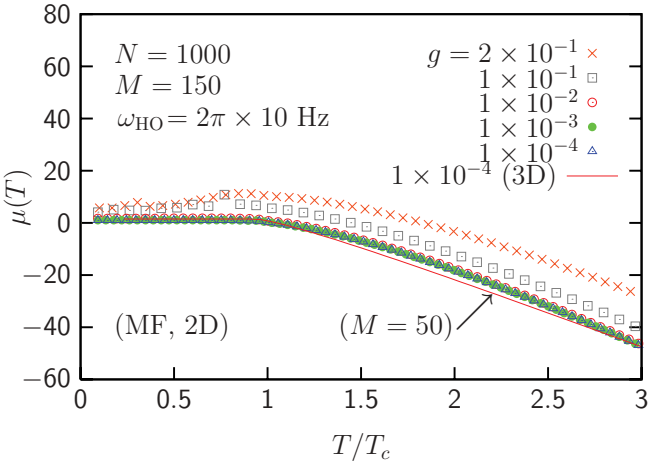

FIG. 9. (Color online) MF chemical potential $\mu(T)$ vs. T for the same system of Fig. 1. The same legends are used as in Fig. 1; but with additional Xs for $g = 2 \times 10^{-1}$, and the solid line for the 3D result at $g = 1 \times 10^{-4}$ and $M = 50$. $\mu(T)$ is in units of $\hbar\omega_{HO}$.

to $T/T_c = 3$ almost matches the 3D result (solid line, $M = 50$) in the weakly interacting regime, although the two results most likely will deviate significantly beyond $T/T_c = 3$. The two-dimensional $\mu(T)$, however, lies slightly higher than the 3D $\mu(T)$ between $T/T_c \approx 1.2$ and ≈ 2.7.

B. Energies

Figure 10 displays the MF energy E_{total} [Eq. (23) multiplied by $\hbar\omega_{HO}/(Nk_BT_c)$] versus T for a two-dimensional, trapped, HS interacting Bose gas of $N = 1000$ particles, $M = 150$ HO states, and trapping frequency $\omega_{HO} = 2\pi \times 10$ Hz. The systems are some of the same contained in Fig. 1. [Note the new label $g = 1 \times 10^0$ (times).] The crosses display what happens when α is not allowed to vary with T and instead is kept constant at 1 for $g = 1.0$. The upper frame displays the temperature range from $T/T_c = 0$ to $T/T_c = 3$. The lower frame is a magnification of the upper frame for $T \leqslant T_c$ only and is presented for a closer inspection of the lower T (condensate) regime. The dashed line in the upper frame displays the analytical result for the classical limit, and the solid line in the lower frame the analytical result for the condensate regime, both given by Pethick and Smith [22]:

$$\frac{E}{Nk_BT_c} = \begin{cases} 2\dfrac{\xi(3)}{\xi(2)}\left(\dfrac{T}{T_c}\right)^3 & : \quad T \leqslant T_c \\ 2\left(\dfrac{T}{T_c}\right)\left[1 - \dfrac{\xi(2)}{2^3}\left(\dfrac{T}{T_c}\right)^2\right] & : \quad T > T_c, \end{cases} \tag{38}$$

where $\xi(3) = 1.202$ and $\xi(4) = 1.645$. The parameter γ of the "weighting function" (24) was set to 0.5 in order for our energies to catch up with the energies of Eq. (38) in the classical regime.

If α is not allowed to vary, i.e., if the wave function (1) is used instead of (3), the thermal behavior of the total energy begins to follow an unphysical character. First, the energy displays an unphysical minimum at some T, beyond which it begins to rise again. Second, the energy is very much overestimated in this T regime for $g = 1.0$. One can therefore see the importance of allowing the wave function to be flexible via a variational parameter, particularly for the strongly interacting regime. Using a flexible wave function, our energies for $T \leqslant T_c$ match the analytical result very closely in the weakly interacting (condensate) regime even up to $g = 0.1$, as displayed in the lower frame of Fig. 10, and are almost insensitive to changes in g.

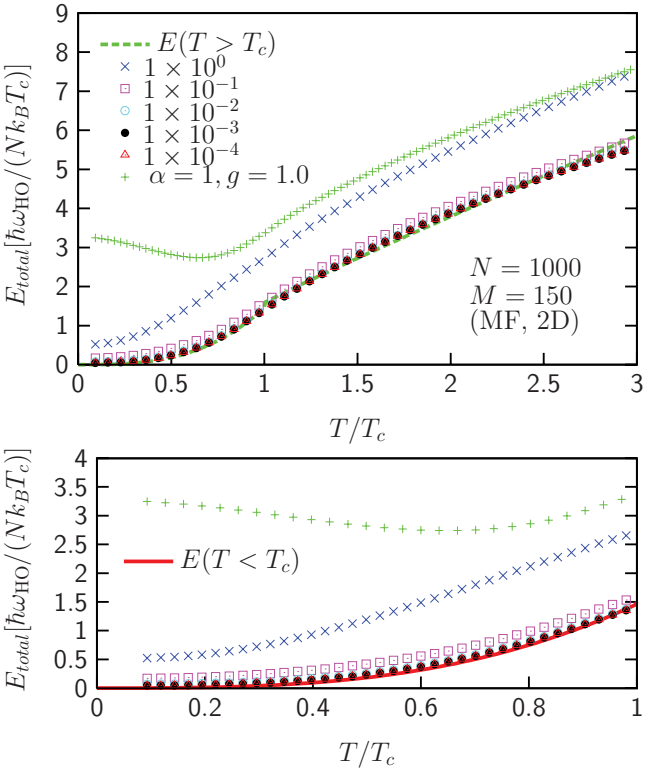

FIG. 10. (Color online) Average MF energy per particle, E_{total} [multiplied by $\hbar\omega_{HO}/(Nk_BT_c)$], for a system of $N = 1000$ particles, $M = 150$ states, and the given g compared to analytical results from Pethick and Smith [22]: The dashed line (slightly hidden behind the solid squares) in the upper frame is the result for $T > T_c$, and the solid line in the lower frame the result for $T \leqslant T_c$, both evaluated by Eq. (38). The radial trapping frequency is $\omega_{HO} = 2\pi \times 10$ Hz. (Xs) $g = 1.0$, very strong interaction; (open squares) $g = 1 \times 10^{-1}$; (open circles) $g = 1 \times 10^{-2}$; (solid circles) $g = 1 \times 10^{-3}$; and (open triangles) $g = 1 \times 10^{-4}$. The crosses reveal the energies evaluated with α being held fixed at 1 for $g = 1.0$. The lower frame is a magnification of the upper frame for $T \leqslant T_c$ only. The energies $E_{\text{total}}[\hbar\omega_{HO}/(Nk_BT_c)]$ are unitless.

In the very strongly interacting regime, $g > 1 \times 10^{-1}$, the energies begin to deviate considerably from the noninteracting result. However, we do not observe the "bump" in the energies as in Ref. [14]. For $g = 1$ (crosses), our energies at $T > T_c$ lie notably higher than the classical limit. Thus, for weak interactions, our MF model with a variational parameter reproduces the energies quite accurately in the condensate regime ($T \leqslant T_c$).

Figure 11 displays the MF energies $E_{\text{total}}[\hbar\omega_{HO}/(Nk_BT_c)]$ for systems of the given N and the same $g = 1 \times 10^{-2}$, $M = 150$, and $\omega_{HO} = 2\pi \times 10$ Hz [(Solid squares) $N = 100$, (open circles) 300, (solid circles) 500, (open triangles) 700,

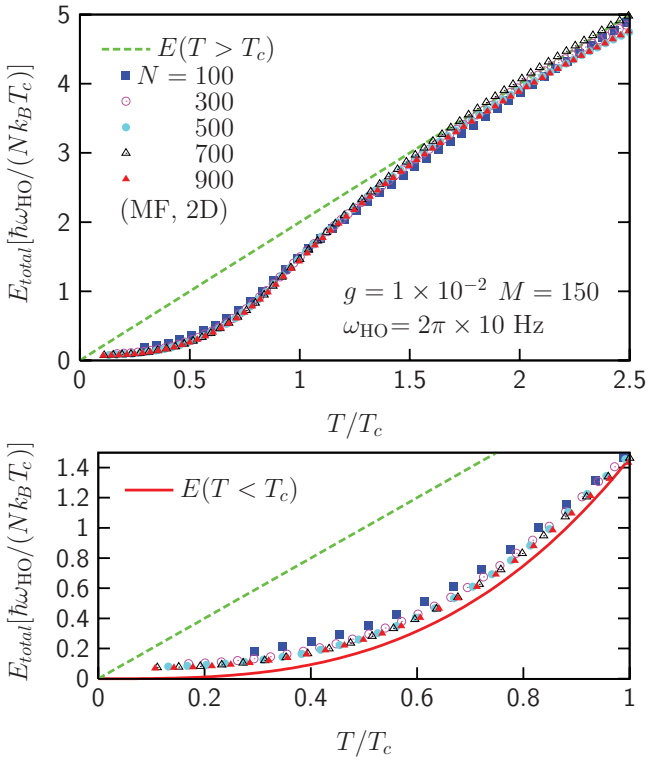

FIG. 11. (Color online) Average MF energy $E_{\rm total}$ [multiplied by $\hbar\omega_{\rm HO}/(Nk_BT_c)$] for a two-dimensional trapped HS Bose gas with $g = 1 \times 10^{-2}$, $M = 150$ states, $\omega_{\rm HO} = 2\pi \times 10$ Hz, and different N. (Solid squares) $N = 100$; (open circles) $N = 300$; (solid circles) $N = 500$; (open triangles) $N = 700$; and (solid triangles) $N = 900$. The dashed line in the upper frame is the classical result at $T > T_c$, and the solid line in the lower frame is for $T \leqslant T_c$ as given by Pethick and Smith [22], Eq. (38). The lower frame is a magnification of the upper frame for $T \leqslant T_c$ only. The energies $E_{\rm total}[\hbar\omega_{\rm HO}/(Nk_BT_c)]$ are unitless.

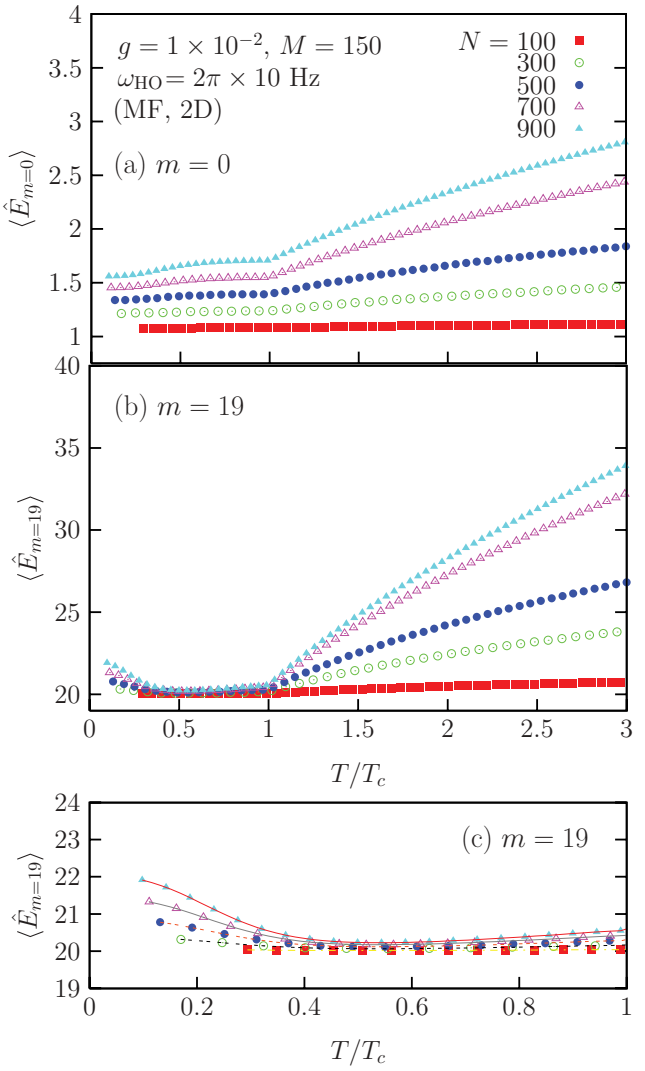

FIG. 12. (Color online) Average MF energy per particle of HO state m, $\langle \hat{E}_m \rangle$, as a function of T for the same systems in Fig. 11. The same legends are used as in Fig. 11. (a) Energies for HO state $m = 0$; (b) HO state $m = 19$ for the same systems of frame (a); and (c) magnified view of frame (b) for $T \leqslant T_c$ only.

and (solid triangles) 900]. In the following figures containing different N, the same latter legends are used. The upper frame is for $0 \leqslant T/T_c \leqslant 2.5$; whereas the lower frame is a magnification of the upper frame for $0 \leqslant T/T_c \leqslant 1$ only. The energies are almost insensitive to changes in N in the given range.

The discreteness of the model described in Sec. II allows us to obtain the energies for each HO state m. Figure 12 displays $\langle \hat{E}_m \rangle / N$ for two arbitrarily chosen m as a function of T for the same systems of Fig. 11. Figure 12(a) displays the results for HO state $m = 0$, Fig. 12(b) that for $m = 19$, and Fig. 12(c) is a magnification of Fig. 12(b) for $T \leqslant T_c$ only.

Figure 12 reveals how the energy for state $m = 0$ rises up to a certain temperature, becomes constant up to $T = T_c$, and then kinks to higher energies. The energies for state $m = 19$, on the other hand, decrease with increasing T from 0 to $\sim 0.5T_c$ but then kink at T_c and rise again with T. This kink becomes more pronounced as the number of particles N rises and is almost absent for a low number, such as $N = 100$. This may indicate the absence of a phase transition for low N. The latter kink is artificial and results from the function $w(T)$ [Eq. (24)] suddenly switching from 1 to $(T/T_c)^\gamma$. This causes the discontinuity in the specific heat capacity in Fig. 16. (It is known that there is indeed a discontinuity in C_v for bosons in two-dimensional harmonic traps [23].) The transition is thus governed by a sudden change in the thermal behavior of the system, i.e., the wave function. The occupancy of each state $\langle \hat{N}_k \rangle$ seems to play a major role in the behavior of $\langle \hat{E}_m \rangle$ up to $T = T_c$. The lower energy levels become sparsely occupied at higher temperatures, causing $\langle \hat{N}_k \rangle$ to drop substantially. As a result, the first term on the right-hand side of Eq. (22) takes over; and since α becomes constant at higher T, as displayed in Fig. 1, the energies $\langle \hat{E}_m \rangle$ reach a plateau toward $T = T_c$. Figure 13 displays $\langle \hat{E}_m \rangle$ for some systems of Fig. 10 with the same labels for the same N and different g indicated. Figures 13(a), 13(b), and 13(c) display the same HO states as in Fig. 12. (Figure 13(a) is in $\log_{10}$ scale.) The energy of the ground state $\langle \hat{E}_{m=0} \rangle$ seems to rise significantly with increasing g. A notable feature is the energy minimum of HO state $m = 19$ for $g = 1 \times 10^{-1}$ observed in frame (b) (open squares).

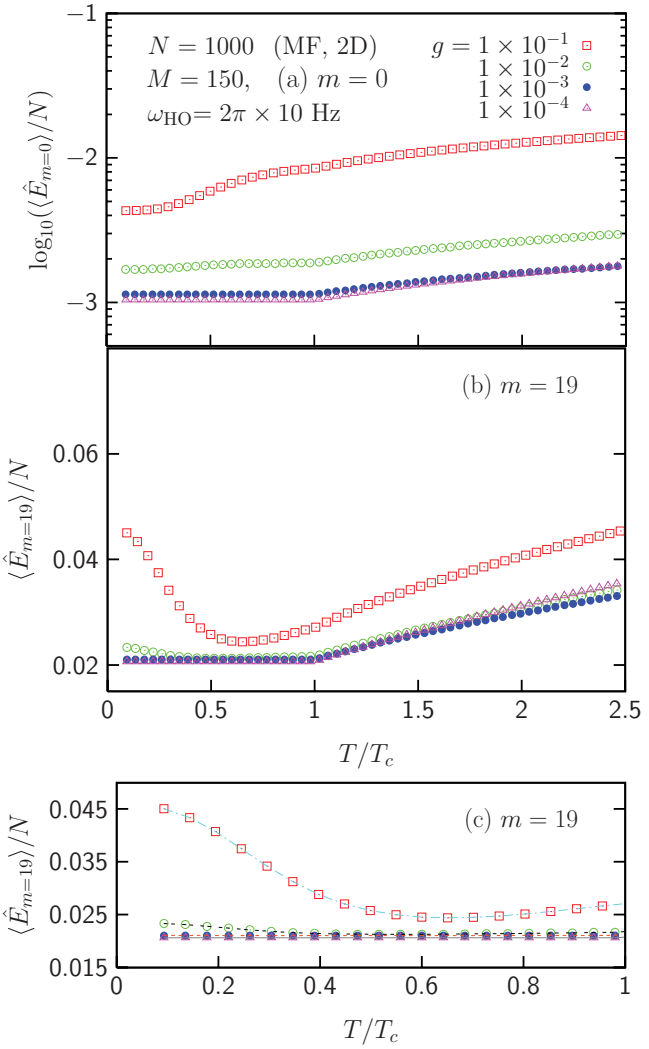

FIG. 13. (Color online) Average MF energy per particle for HO state m, $\langle \hat{E}_m \rangle$, for the same system of Fig. 1 at the given values of g. The legends are as in Fig. 1. (a) HO state $m = 0$ ($\log_{10}$ scale, ground state); (b) HO state $m = 19$ for the same systems of (a); (c) magnified view of (b) in the regime $T \leqslant T_c$. $\langle \hat{E}_m \rangle$ is in units of $\hbar\omega_{HO}$.

C. Occupancies

Figure 14 displays occupancies $\langle \hat{N}_{n=0} \rangle$ [Eq. (17)] as a function of T for the same systems of Fig. 13 at the given values of g. We also display the 3D result (crosses) from Ref. [11] for the same N and ω_{HO} but using $M = 45$ states. One can see that, even as g becomes large (0.1), the occupancy $\langle \hat{N}_0 \rangle / N$ does not reveal any change in its profile. The reason is because our mean-field model is very simplistic and hence has its limitations as any other mean-field model. Whereas, on the one hand, our model reproduces the mean-field energies we need for the SFA very well as we demonstrated in Figs. 10 and 11, the model is unable, on the other hand, to reproduce the condensate depletion, particularly in the strongly interacting regime. The reason is because when g is increased, the parameter α decreases as can be deduced from Eq. (26) and Fig. 1. That is to say, these two parameters compete with each other, such as can be seen in Eq. (22), where there is

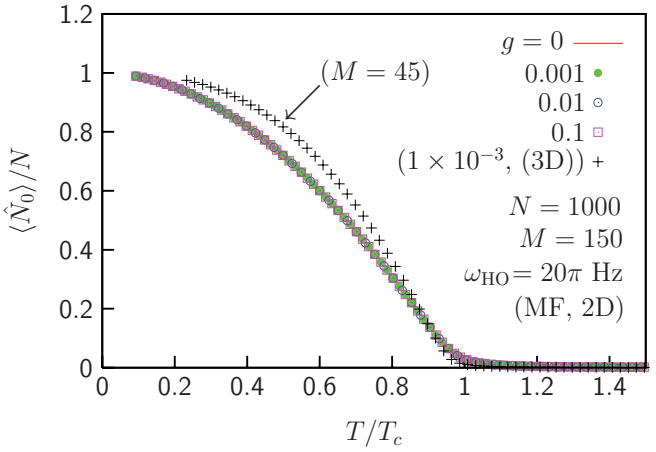

FIG. 14. (Color online) Average MF fractional occupancy of state $m = 0$, $\langle \hat{N}_0 \rangle / N$, as a function of T for the same systems as in Fig. 1 at the given values of g. The same legends are used as in Fig. 13, with additional crosses for the three-dimensional result at $g = 1 \times 10^{-3}$ and the solid line for the noninteracting case $g = 0$.

the coefficient $g\alpha$ in the interacting part of the energy. We would like then to argue that we are aware of this fact but that we are nevertheless able to demonstrate condensate depletion by "artificially" disallowing a variational optimization of the wave function in a special figure (Fig. 15) for the occupancies. The latter displays $\langle \hat{N}_0 \rangle / N$ at the indicated values of g for the same 2D system of Fig. 14 but with α held fixed at 1 for all temperatures. But we must remind the reader that our goal is not to explore the condensate depletion but rather the thermodynamic properties which are reproduced largely in the bulk of this article. Thus, Fig. 15 very much speaks for itself: in the absence of a variational optimization, condensate depletion can be obtained by increasing g; however, the width of the wave function remains the same. Finally, the depletion in Fig. 14 is more pronounced for the two-dimensional system than for the three-dimensional case of Ref. [11]. Thus,

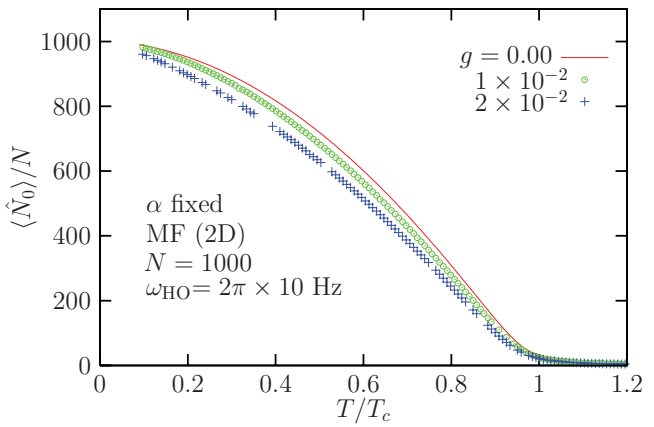

FIG. 15. (Color online) Demonstration of artificial condensate depletion via the occupancies $\langle N_0 \rangle / N$ in the absence of variational optimization. The variational parameter α is fixed to 1. The system is a 2D harmonically trapped Bose gas of $N = 1000$ particles at a trapping frequency of $\omega_{HO} = 2\pi \times 10$ Hz. (Solid line) Occupancy in the noninteracting case $g = 0$; (open circles) $g = 0.01$; (crosses) 0.02.

reducing the dimensions of the system (i.e., increasing the confinement) enhances the depletion of the $m = 0$ condensate in the low-temperature regime.

D. Thermodynamic properties

To evaluate the thermodynamic properties, we used the SFA in 2D. This is the first time that the SFA is used to explore a 2D trapped system. The SFA method was outlined previously [11] and we shall not explain it again. Its two-dimensional reformulation is pretty much straightforward. In passing, we shall shed more light on the effect of interactions and number of particles on the thermodynamic properties of two-dimensional trapped HS Bose gases.

1. Specific heat capacity

Figure 16 displays the specific heat capacity per particle, $C_v/(Nk_B)$, where k_B is Boltzmann's constant, for a system of $N = 1000$, $M = 150$, and $\omega_{\rm HO} = 2\pi \times 10$ Hz, at several values of g. The systems are the same as in Fig. 3. The three-dimensional result of Ref. [11] for $g = 1 \times 10^{-4}$ and $M = 45$ is also displayed (solid line). The dashed line is the analytical result of Grether *et al.* [24] given by

$$\frac{C_v}{Nk_B} = \frac{(d+\delta)}{2}\left(\frac{d+\delta}{2}+1\right)\left(\frac{T}{T_c}\right)^{(d+\delta)/2}\frac{g_{(d+\delta)/2+1}(1)}{g_{(d+\delta)/2}(1)} \tag{39}$$

for $T \leqslant T_c$, and

$$\frac{C_v}{Nk_B} = \frac{(d+\delta)}{2}\left[\left(\frac{d+\delta}{2}+1\right)\frac{g_{(d+\delta)/2+1}(z_1)}{g_{(d+\delta)/2}(z_1)} - \frac{d+\delta}{2}\frac{g_{(d+\delta)/2}(z_1)}{g_{(d+\delta)/2-1}(z_1)}\right] \tag{40}$$

for $T > T_c$. Note that our $C_v/(Nk_B)$ matches that of Grether *et al.* closely, except in the neighborhood of T_c. That sharp feature of the transition is missing in our case. Instead, our result displays a discontinuity at T_c which arises from the kinks in the energies at T_c displayed in Figs. 12 and 13. It is possible that the SFA energy fluctuations were able to soften the transition of our C_v at T_c. The two-dimensional result lies lower than the three-dimensional result. The transitional peak is higher in 3D than in 2D. We note that the three-dimensional C_v was plotted against T/T_c with T_c for the three-dimensional result (4.5113 nK) and the two-dimensional C_v with T_c for the two-dimensional result (11.833 nK). This approach is followed in the rest of the figures comparing to three-dimensional results. In addition, similarly to our findings in Ref. [11] for the three-dimensional case, the two-dimensional C_v does not seem to change very much with g in the weakly interacting regime. However, when g is held constant and N is changed, it is found that the response of C_v is stronger to changes in N than changes in g. The same conclusions apply to the case of fixed g and varying N in Ref. [11]. Figure 17 displays the latter case for the same systems of Fig. 12 at $g = 1 \times 10^{-2}$, $M = 150$, and the given values of N. Here T_c is fixed at 11.83 nK. Figure 17 shows that there is absolutely no peak for lower N, such as 100. Thus, it seems that, for low N, there is no BEC transition into the $m = 0$ HO state.

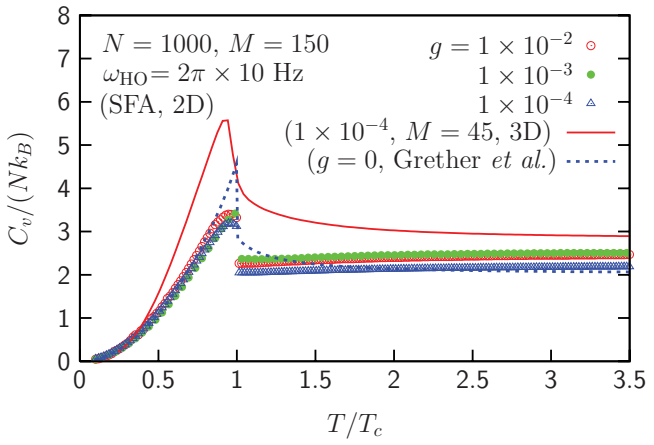

FIG. 16. (Color online) SFA specific heat capacity C_v as a function of temperature for the same systems of Fig. 3. The solid line is for the three-dimensional result at $g = 1 \times 10^{-4}$ and $M = 45$. The same legends are used as in Fig. 3. $C_v/(Nk_B)$ is unitless.

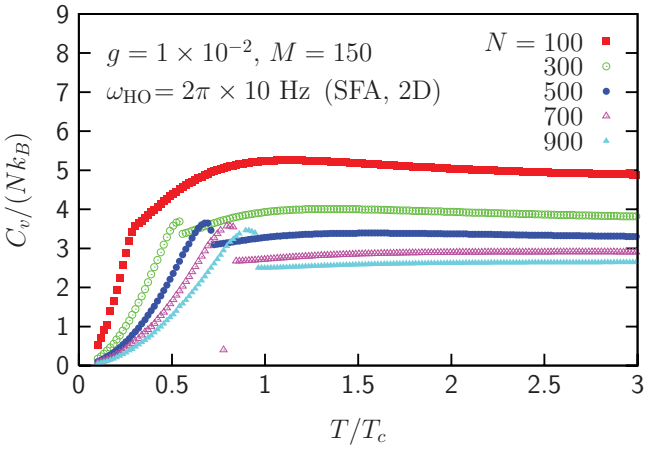

FIG. 17. (Color online) SFA specific heat capacity C_v in units of Nk_B for the same systems of Fig. 12.

2. Internal energy

Figures 18 and 19 display the same cases as Figs. 16 and 17, respectively, but for the internal energy per particle $\langle U\rangle/N$. The dashed line is the analytical result of Grether *et al.* [24] given by

$$\frac{U}{N} = \frac{\hbar\omega_{\rm HO}\delta}{2} + \frac{(d+\delta)}{2}\frac{g_{(d+\delta)/2+1}(z_1)}{g_{(d+\delta)/2}}\frac{1}{\beta}, \tag{41}$$

with $z_1 = \exp[\beta(\mu - \delta\hbar\omega_{\rm HO}/2)]$, $\delta = 2$, $d = 2$, and $g_n(z_1)$ the Bose function. The SFA result matches almost exactly the analytical result of Grether *et al.* in the weakly interacting regime. Again, the same features are observed: $\langle U\rangle/N$ in the range of g considered shows only little response to changes in g and responds strongly to changes in N. The three-dimensional result at $g = 1 \times 10^{-4}$ from Ref. [11] is included in Fig. 18 here as well (solid line). One observes that the two-dimensional case yields larger internal energies than in 3D. For example, at $T = 3T_c$ in Fig. 18, $\langle U\rangle/N \sim 150$; whereas the three-dimensional case yields ~75. In addition, Fig. 18 of Ref. [11] displays a kink in $\langle U\rangle$ vs. T; whereas in

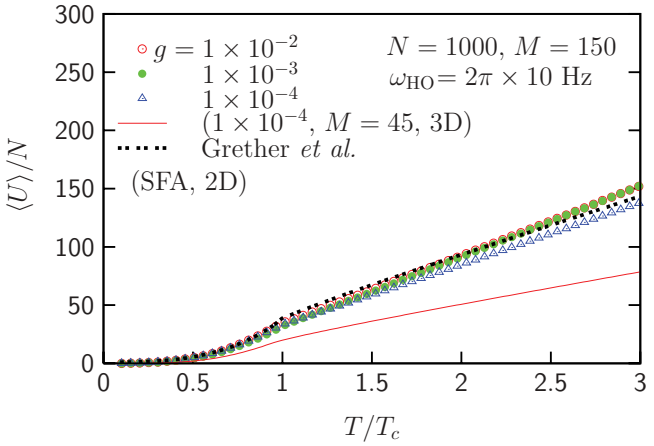

FIG. 18. (Color online) SFA average internal energy per particle $\langle U \rangle / N$ as a function of temperature for the same systems (with the 3D result) of Fig. 16. (Dashed line) Analytical result due to Grether *et al.* [24]. The same legends are used as in the latter figures. $\langle U \rangle$ is in units of $\hbar\omega_{HO}$.

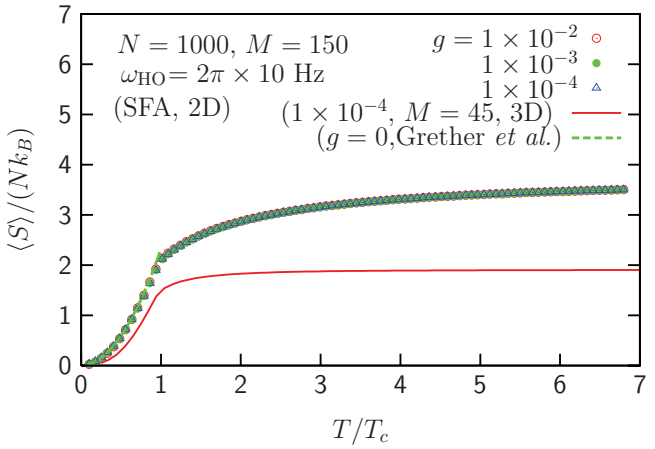

FIG. 20. (Color online) SFA average entropy $\langle S \rangle$ as a function of temperature for the same systems of Fig. 16 plus the three-dimensional result. (Dashed line) Analytical result for $T \leqslant T_c$ from Grether *et al.* [24]. The same legends are used as in Fig. 16. $\langle S \rangle / (Nk_B)$ is unitless.

Figs. 18 and 19 here this kink is absent. It can therefore be concluded that the 2D confinement yields an increase in the internal energy.

3. *Entropy*

As before, Figs. 20 and 21 display the entropy per particle $\langle S \rangle / (Nk_B)$ for our previous systems considered in Figs. 16 and 17, respectively. The dashed line shows the analytical result of Grether *et al.* [24] for $T \leqslant T_c$ given by

$$\frac{S}{Nk_B} = \left[\frac{(d+\delta)}{2} + 1\right] \left(\frac{T}{T_c}\right)^{(d+\delta)/2} \frac{g_{(d+\delta)/2+1}(1)}{g_{(d+\delta)/2}(1)}. \quad (42)$$

Here we have used $d = \delta = 2$, $T_c = 1.1833 \times 10^{-8}$ K, and $g_n(1)$ is the Bose function at 1, where n is an integer. Our SFA entropy for $T \leqslant T_c$ matches that of Grether *et al.* exactly. This proves that SFA reproduces the entropy accurately in the weakly interacting regime at $T \leqslant T_c$. The three-dimensional result at $g = 1 \times 10^{-4}$ and $M = 45$ from Fig. [21] of Ref. [11] is included in Fig. 20 (solid line). The three-dimensional case yields a lower entropy than the corresponding two-dimensional case. Hence one can conclude that a much lower order exists in the three-dimensional case than the two-dimensional one. Further, we note that $\langle S \rangle$ rises initially up to $T = T_c$ but then begins to flatten out as in the three-dimensional case. It seems also insensitive to changes in g within the range considered and responds strongly to variations in N.

4. *Pressure*

One of the thermodynamic properties rarely mentioned in the literature on Bose gases in traps is the pressure. Here we are able to evaluate it as a function of temperature. Figures 22 and 23 display the pressure $\langle P \rangle$ vs. T for the previous systems in Figs. 16 and 17, respectively. Figure 22 displays a slight kink in $\langle P \rangle$ at $T \sim T_c$ and $\langle P \rangle$ rises almost linearly after $T = T_c$. The pressure is again unaffected by variations in g and responds strongly to variations in N. Further, the pressure in Fig. 22 is

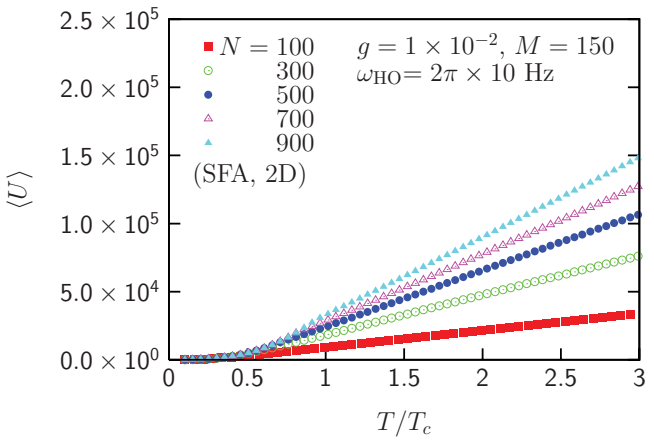

FIG. 19. (Color online) SFA average internal energy $\langle U \rangle$ as a function of temperature for the same systems of Fig. 17. The same legends are used as in Fig. 11. $\langle U \rangle$ is in units of $\hbar\omega_{HO}$.

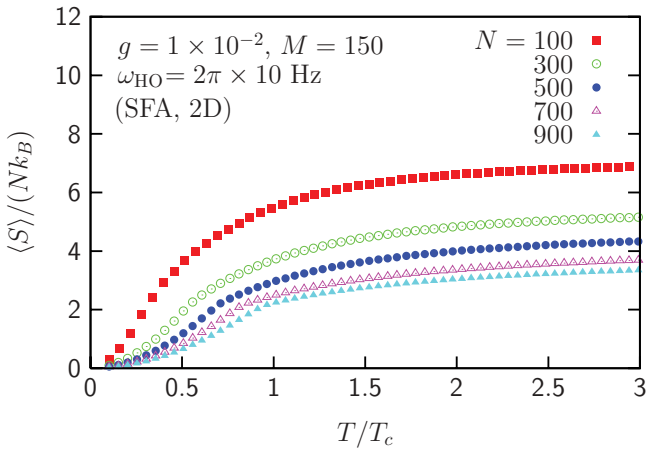

FIG. 21. (Color online) SFA average entropy $\langle S \rangle$ as a function of temperature for the same systems of Fig. 17. The same legends are used as in Fig. 17. $\langle S \rangle / (Nk_B)$ is unitless.

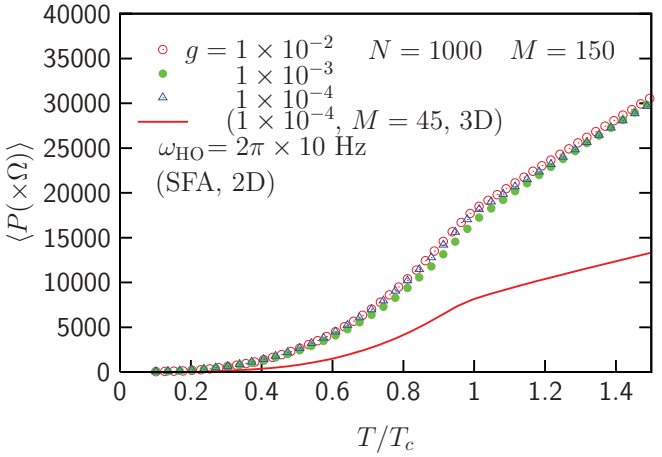

FIG. 22. (Color online) SFA average pressure $\langle P\rangle$ $(\times\Omega)$, where Ω is the volume of the system, as a function of temperature for the same systems of Fig. 16 (with the three-dimensional result included). The same legends are used as in Fig. 16. $\langle P\rangle$ $(\times\Omega)$ is in units of $\hbar\omega_{HO}$.

larger than the three-dimensional case (solid line) by a factor of ~2 at $T/T_c = 1.5$. The two-dimensional confinement thus enhances the pressure.

E. Number fluctuations

In what follows, we display the behavior of the SFA number fluctuations $\langle(\Delta\hat{N}_m)^2\rangle$ as a function of temperature. The goal is to delve deeper into the characteristics of the discrete structure of the current model.

Figure 24 displays an overview of the thermal behavior of the number fluctuations $\langle(\Delta\hat{N}_m)^2\rangle$ [Eq. (31)] for a large number of states m, beginning with $m = 1$, the first excited state from Fig. 24(a) and then going down sequentially to state $m = 147$ in Fig. 24(d). The system is a two-dimensional, trapped, HS Bose gas of $N = 1000$ particles and $g = 1 \times 10^{-3}$. Some interesting features are revealed. $\langle(\Delta\hat{N}_1)^2\rangle$ displays two peaks at $T \sim 0.5T_c$ and $\sim 0.9T_c$. As one goes to higher states m, these peaks begin to disappear at $m = 3$. Beyond T_c $\langle(\Delta\hat{N}_m)^2\rangle$

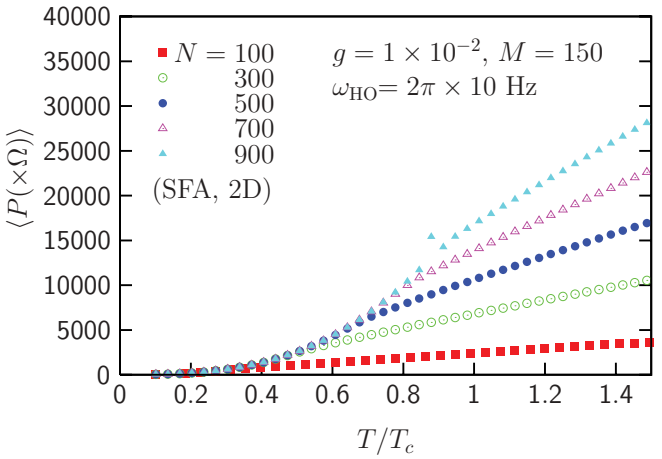

FIG. 23. (Color online) SFA average pressure $\langle P\rangle$ $(\times\Omega)$ for the same systems of Fig. 17. The same legends are used as in Fig. 17. $\langle P\rangle$ $(\times\Omega)$ is in units of $\hbar\omega_{HO}$.

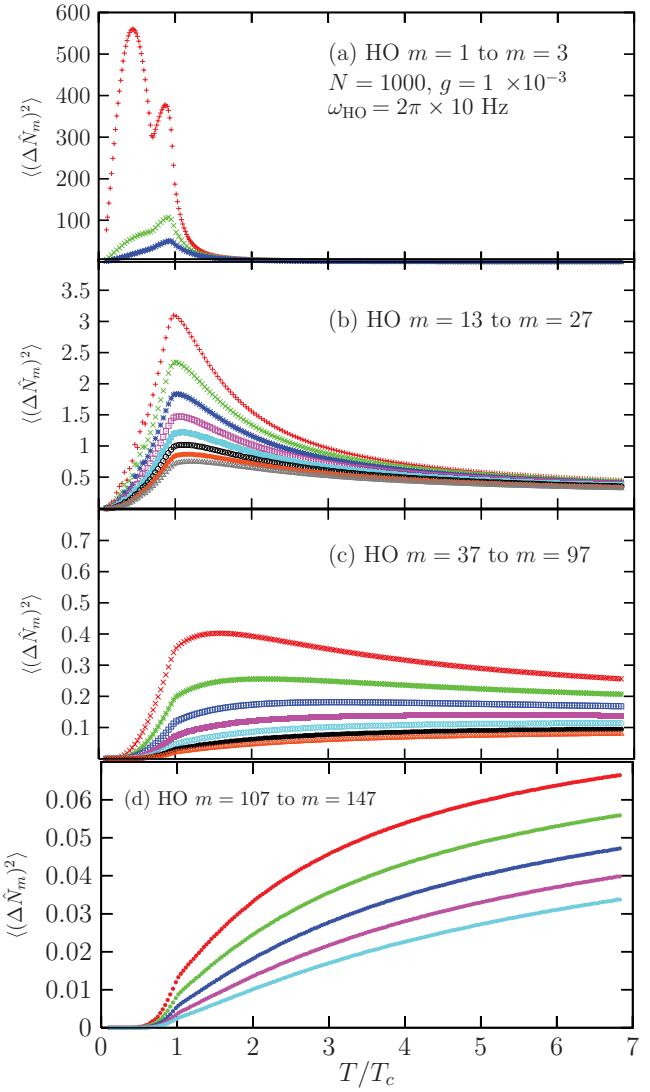

FIG. 24. (Color online) Overview of the SFA average number fluctuations, $\langle(\Delta\hat{N}_m)^2\rangle$, for the given HO states m vs. temperature. The system is a trapped HS Bose gas of $N = 1000$ particles and $g = 1 \times 10^{-3}$. (a) HO states $m = 1$ to 3; (b) $m = 13$ to 27 in steps of 2; (c) $m = 37$ to 97, again in steps of 10; (d) similarly, again for $m = 107$ to 147 in steps of 10.

decays down to zero, apparently only for the lower-lying states $m < 10$. For the states $m = 13$ up to 27 (in steps of 2), $\langle(\Delta\hat{N}_m)^2\rangle$ displays a universal maximum at T_c, beyond which the fluctuations decay. They nevertheless still have some significant value at $T \sim 7T_c$. For states $m = 37$ up to 97 (again in steps of 10), the behavior of $\langle(\Delta\hat{N}_m)^2\rangle$ begins to change toward a lower decay rate beyond T_c, until at, say $m = 107$ to 147 (steps of 10), $\langle(\Delta\hat{N}_m)^2\rangle$ actually rises only with increasing T and does not decay. It can be further seen that $\langle(\Delta\hat{N}_m)^2\rangle$ in general decreases with increasing m.

V. DENSITY MATRIX OF HARMONIC OSCILLATOR ORBITALS

In this section, we show the density matrices arising from the correlations between some of the HO states. The goal is to

make further use of the wave function (3) involving discrete energy levels and extract further information from it, such as the strength of the correlations via the density matrix. The density matrix can be defined by

$$\rho(\mathbf{r},\mathbf{r}';\alpha) = \langle\hat{\psi}^{\dagger}(\mathbf{r},\alpha)\hat{\psi}(\mathbf{r}',\alpha)\rangle. \tag{43}$$

Substituting

$$\hat{\psi}(\mathbf{r},\alpha) = \sum_{m}\hat{b}_m\phi_m(\mathbf{r},\alpha), \tag{44}$$

with

$$\phi_m(\mathbf{r},\alpha) = \phi_{m_x}(x,\alpha)\phi_{m_y}(y,\alpha) \tag{45}$$

into Eq. (43) for the two-dimensional case, we get

$$\rho(\mathbf{r},\mathbf{r}';\alpha) = \sum_{m_x,m_y,n_x,n_y}\phi_{m_x}(x,\alpha)\phi_{m_y}(y,\alpha) \times \phi_{n_x}(x',\alpha)\phi_{n_y}(y',\alpha)\langle\hat{N}_m\rangle\delta_{n_x+n_y,m_x+m_y}, \tag{46}$$

under the condition that $n_x+n_y=m_x+m_y=m$, where $\phi_{m_x}(x,\alpha)$ is given by Eq. (3). Thus, the amplitude of the density matrix is determined by the weight $\langle\hat{N}_m\rangle$. It is interesting to examine the individual components of $\rho(\mathbf{r},\mathbf{r}';\alpha)$, that is, the different combinations of the m_x,m_y,n_x, and n_y orbitals. For this purpose, we define

$$\rho_{m_x,m_y,n_x,n_y}(\mathbf{r},\mathbf{r}';\alpha) = \phi_{m_x}(x,\alpha)\phi_{m_y}(y,\alpha) \times \phi_{n_x}(x',\alpha)\phi_{n_y}(y',\alpha)\langle\hat{N}_{m=m_x+m_y}\rangle \times \delta_{n_x+n_y,m_x+m_y}, \tag{47}$$

with $\mathbf{r}=x\mathbf{i}+y\mathbf{j}$ and $\mathbf{r}'=x'\mathbf{i}+y'\mathbf{j}$ and plot some of them in Figs. 25–29. Figure 25 displays $\rho_{1111}(\mathbf{r},\mathbf{r}';\alpha)$ at $T=3.81\times10^{-8}$ K, signaling the correlations of first-excited HO modes with themselves. The temperature here is not very important, since it only determines the weight $\langle\hat{N}_m\rangle$ and not the structure. Except for the rectangular-like patches on the density surface, $\rho_{1111}(\mathbf{r},\mathbf{r}';\alpha)$ is largely zero. Obviously, the correlations are only significant for certain values of $\mathbf{r}$ and $\mathbf{r}'$ lying within those patches. The zero values of the density correspond to $H_1(x)$ becoming zero at $x=0$ and similarly for the rest of the coordinates. This means that correlations with particles in the first-excited state positioned along one of the coordinate axes is entirely zero for this density matrix.

Figure 26 displays $\rho_{40,2,40,2}(\mathbf{r},\mathbf{r}';\alpha)$ at the same temperature as in Fig. 25. A wavy, sinusoidal-like structure is observed with hills and valleys. The amplitude of this structure is very low,

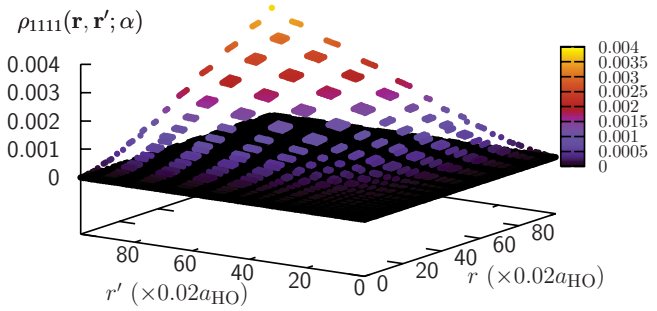

FIG. 25. (Color online) Density matrix of the $m_x=1$, $m_y=1$, $n_x=1$, and $n_y=1$ HO modes, $\rho_{1111}(\mathbf{r},\mathbf{r}';\alpha)$.

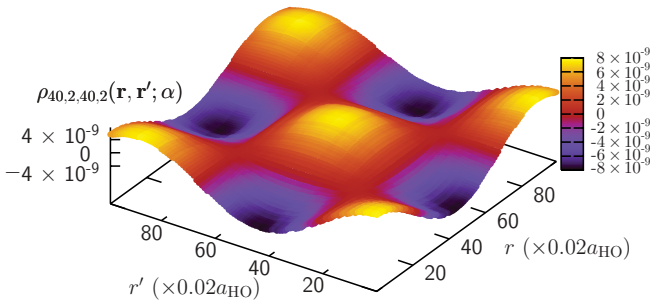

FIG. 26. (Color online) Density matrix of the $m_x=40$, $m_y=2$, $n_x=40$, and $n_y=2$ HO modes, $\rho_{40,2,40,2}(\mathbf{r},\mathbf{r}';\alpha)$.

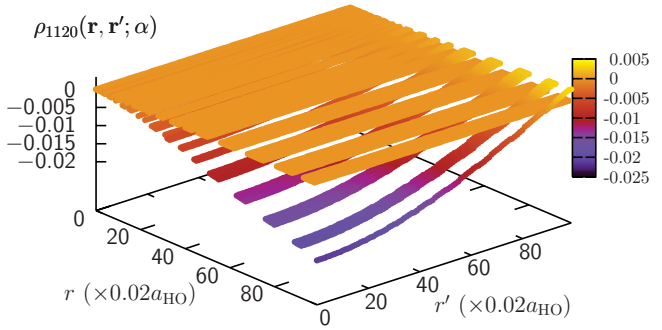

FIG. 27. (Color online) Density matrix of the $m_x=1$, $m_y=1$, $n_x=2$, and $n_y=0$ HO modes, $\rho_{1120}(\mathbf{r},\mathbf{r}';\alpha)$.

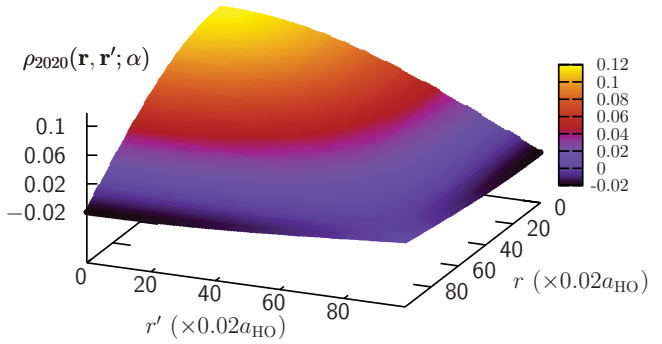

FIG. 28. (Color online) Density matrix of the $m_x=2$, $m_y=0$, $n_x=2$, and $n_y=0$ HO modes, $\rho_{2020}(\mathbf{r},\mathbf{r}';\alpha)$.

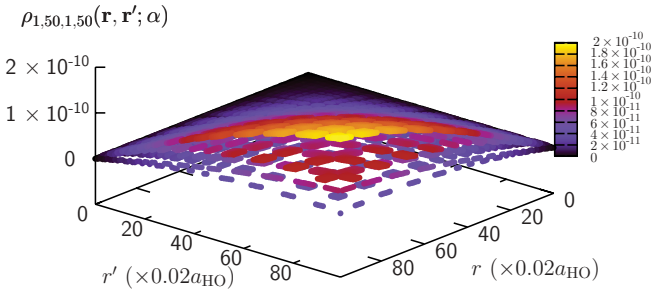

FIG. 29. (Color online) Density matrix of the $m_x=1$, $m_y=50$, $n_x=1$, and $n_y=50$ HO modes, $\rho_{1,50,1,50}(\mathbf{r},\mathbf{r}';\alpha)$.

indicating that the correlations between low- and high-lying HO states such as 2 and 40 are very weak (order $\sim 10^{-9}$), as can be seen from the figure. On the other hand, a striped structure is obtained on plotting $\rho_{1120}(\mathbf{r},\mathbf{r}';\alpha)$, as displayed in Fig. 27. It seems that rectangular patches or stripes arise in the density matrix whenever one of the HO states is 1. Further, it seems that the presence of the zeroth-HO state $\phi_0(y',\alpha)$ in

$$\rho_{1120}(\mathbf{r},\mathbf{r}';\alpha) = \phi_1(x,\alpha)\phi_1(y,\alpha)\phi_2(x',\alpha)\phi_0(y',\alpha) \quad (48)$$

causes the density to remain continuous along r', whereas along r it becomes discontinuous. Note that ρ_{1120} forms areas of zero-correlation stripes. Further, a smooth, almost planar, surface is observed for $\rho_{2020}(\mathbf{r},\mathbf{r}';\alpha)$, displayed in Fig. 28. This seems to arise due to the connection to the HO ground state. The correlations here are much larger than in any of the previous figures. Figure 29 displays $\rho_{1,50,1,50}(\mathbf{r},\mathbf{r}';\alpha)$ with a patched structure similar to Fig. 25, except that there are several layers for these patches.

VI. DISCUSSION AND CONCLUSIONS

In summary, then, we presented an application of the SFA to the evaluation of the thermodynamic properties of a two-dimensional, trapped, HS Bose gas and provided a comprehensive examination of these properties. The energies necessary for the SFA were obtained by a mean-field model which reproduced the energies of the system reasonably well in the HO condensate regime but required some artificial adjustment in order to reproduce the energies in the high-temperature classical regime. However, our goal was not to calculate energies; the present approach can be viewed as a simple method to obtain the energy for each HO state m. The SFA technique used here had been employed earlier for the three-dimensional trapped HS Bose gas [11]. Once again, the SFA provided stable solutions to the fluctuations of the energy, even after only a small number of iterations. The advantage of the SFA was demonstrated in that it reproduced the thermodynamic properties of a 2D harmonically trapped HS Bose gas for a broad range of temperature in one single calculation. However, the SFA failed at very strong interactions as we were not able to go beyond $g = 0.01$. It was found that there were substantial differences between the thermodynamic properties of a trapped HS Bose gas in 2D and 3D. Condensation in the $m = 0$ HO state was obtained but not in the zero-momentum state. The two-dimensional condensate in the $m = 0$ state is depleted more than its three-dimensional counterpart.

A. Weighting function

The necessity for multiplying Eq. (23) by a "weighting function" of the form (24) signals that the wave function (3) needs further development in order to take into account the thermal variations more accurately, particularly in the high-temperature regime. On the other hand, it may also suggest a thermal variation for the interaction parameter g.

B. SFA internal energy

The differences between the two-dimensional and three-dimensional $\langle U\rangle/N$, as revealed by Fig. 18, display that a reduced dimensionality causes a stronger confinement and hence lower degrees of freedom for the bosons. Now, these are only able to move in the xy plane within a circle whose radius is defined by the external harmonic trap. As a result, the rate of the collisions between the particles in 2D is larger than in 3D, causing the internal energy and the pressure to be larger as well.

C. SFA energy fluctuations

An increase in g causes stronger energy fluctuations, which decay with temperature T. Going to even larger values of g, such as 0.1 and beyond, causes SFA to break down again, as in the three-dimensional case. Thus, whereas the SFA provides thermodynamic properties in the weakly interacting regime, it fails to do so for the very strongly interacting regime, $g > 0.01$. The failure happens in the iterative scheme of the procedure. In fact, if one could evaluate the SFA energy fluctuations analytically, without resorting to an iterative procedure, the thermodynamic properties could be evaluated easily in the very strongly interacting regime.

D. MF condensate depletion

The enhancement of the $m = 0$ HO condensate depletion in the two-dimensional case, as compared to the three-dimensional case in Fig. 14, is due to the fact that it is more difficult for bosons to correlate with each other in 2D. That is, the confinement into the xy plane reduces the chance for pair correlations that build the condensate.

E. MF correlations

Figures 25–29 reveal that correlations between even HO states $m > 0$ and the condensate $m = 0$ are strong. However, odd states correlate only weakly with the state $m = 0$. The correlations between high states such as $m = 50$ and low ones, e.g., $m = 1$, are vanishingly small; yet they reveal interesting structures. Further, the correlations between excited states ($m > 0$) themselves follow complicated patterns, as revealed by the complicated structures of the components of the density matrix.

F. Importance

A new projected Gross-Pitaevskii-equation approach was employed by Bezett and Blakie [16] in order to investigate the critical properties of a trapped Bose-Einstein condensate. It was noted that the susceptibility and heat capacity are not easy to measure in atomic gases, and finite-size effects have a profound effect on the critical properties of a system. Hence the importance of the present investigation. If developed further, the SFA can open more doors for the study of the thermodynamic properties of the trapped two-dimensional Bose gas in the strongly interacting regime.

ACKNOWLEDGMENTS

One of us (H.B.G.) is grateful to The University of Jordan for granting him a sabbatical leave, during which the present work was completed under the general title "Many-Body Systems: Further Studies and Calculations (Part Two)."

[1] K. Nho and D. P. Landau, Phys. Rev. A **73**, 033606 (2006).
[2] Anna Posazhennikova, Rev. Mod. Phys. **78**, 1111 (2006).
[3] L. Pricoupenko, Phys. Rev. A **70**, 013601 (2004).
[4] J. L. Song and F. Zhou, Phys. Rev. Lett. **103**, 025302 (2009).
[5] R. N. Bisset and P. B. Blakie, Phys. Rev. A **80**, 035602 (2009).
[6] Stefan Heinrichs and William J. Mullin, J. Low Temp. Phys. **113**, 231 (1998).
[7] Sean Pearson, Tao Pang, and Changfeng Chen, Phys. Rev. A **58**, 4811 (1998).
[8] Christopher Gies, Brandon P. van Zyl, S. A. Morgan, and D. A. W. Hutchinson, Phys. Rev. A **69**, 023616 (2004).
[9] N. M. Ghulam, H. B. Ghassib, and M. K. Al-Sugheir, Phys. Rev. C **75**, 064317 (2007).
[10] R. R. Nigmatullin, A. A. Khamzin, and H. B. Ghassib, Phys. Rev. E **61**, 3441 (2000).
[11] Saleem I. Qashou, Mohamed K. Al-Sugheir, Asaad R. Sakhel, and Humam B. Ghassib, e-print arXiv:1010.3691.
[12] A. R. Sakhel, J. L. DuBois, and H. R. Glyde, Phys. Rev. A **66**, 063610 (2002).
[13] J. L. DuBois and H. R. Glyde, Phys. Rev. A **63**, 023602 (2001).
[14] M. Bayindir and B. Tanatar, Phys. Rev. A **58**, 3134 (1998).
[15] Suboda Mishra and Peter Pfeifer, J. Phys. A: Math. Theor. **40**, F243 (2007).
[16] A. Bezett and P. B. Blakie, Phys. Rev. A **79**, 033611 (2009).
[17] D. S. Petrov, M. Holtzmann, and G. V. Shlyapnikov, Phys. Rev. Lett. **84**, 2551 (2000).
[18] Z. Hadzibabic, P. Krüger, M. Cheneau, S. P. Rath, and J. Dalibard, New J. Phys. **10**, 045006 (2008).
[19] W. J. Mullin, J. Low Temp. Phys. **106**, 615 (1997).
[20] G. E. Astrakharchik, J. Boronat, J. Casulleras, I. L. Kurbakov, and Yu. E. Lozovik, Phys. Rev. A **79**, 051602(R) (2009).
[21] G. B. Arfken and H. J. Weber, *Mathematical Methods for Physicists*, 4th ed. (Academic Press, San Diego, USA, 1995).
[22] C. J. Pethick and H. Smith, *Bose-Einstein Condensation in Dilute Gases*, 1st ed. (Cambridge University Press, Cambridge, UK, 2002).
[23] V. I. Yukalov, Phys. Rev. A **72**, 033608 (2005).
[24] M. Grether, M. Fortes, M. de Llano, J. L. del Río, F. J. Sevilla, M. A. Solís, and A. A. Valladares, Eur. Phys. J. D **23**, 117 (2003).